Universidade de Aveiro Departamento de Física
2009

Wenbin You

Propriedades eléctricas de filmes de nanocristais de Si processados a partir de tintas de Si

Electrical properties of Si nanocrystal films processed from Si-inks

Universidade de Aveiro Departamento de Física
2009

Wenbin You

Propriedades eléctricas de filmes de nanocristais de Si processados a partir de tintas de Si

Electrical properties of Si nanocrystal films processed from Si-inks

Dissertação apresentada à Universidade de Aveiro para cumprimento dos requisitos necessários à obtenção do grau de Mestre em Ciência e Engenharia dos Materiais (EMMS), realizada sob a orientação científica do Dr. Rui Nuno Marques Pereira, Investigador do Departamento de Física da Universidade de Aveiro, e do Prof. Dr. António Ferreira da Cunha, Prof. Auxiliar do Departamento de Física da Universidade de Aveiro.

A dissertation presented to the University of Aveiro for the fulfillment of the requirement to obtain the Master degree in Materials Science and Engineering (EMMS), under the scientific guidance of Dr. Rui Nuno Marques Pereira, Researcher of the Department of Physics of the University of Aveiro, and of Prof. Dr. António Ferreira da Cunha, Assistant Professor of the Department of Physics of the University of Aveiro.

The Board of Examiners

president

Prof. Dr. Vitor Brás de Sequeira Amaral
Associate professor from the University of Aveiro (President)

Dr. Rui Nuno Marques Pereira
Researcher from the University of Aveiro (Supervisor)

Prof. Dr. António Ferreira da Cunha
Assistant Professor from the University of Aveiro (Co-supervisor)

Prof. Dr.-Ing. habil. Jörg Müller
Professor from the Hamburg University of Technology (Co-supervisor)

Dr. Sergej Filonovich
Researcher from the New University of Lisbon (Invited examiner)

Acknowledgements

I express my deepest gratitude to my two supervisors Dr. Rui Nuno Marques Pereira and Prof. António Ferreira da Cunha for their invaluable guidance, support and encouragement throughout this work. I thank them for critical supervision and patient listening of my thoughts. I attribute every progress of this research to their encouragement and efforts and without them this thesis, too, would not have been completed.

I am also extremely grateful to Prof. Jörg Müller, a co-supervisor from Technical University of Hamburg-Harburg (TUHH), who has given me invaluable suggestions and help to finish this master degree.

I offer my sincerest gratitude to all the people who shared their experience and knowledge and made friendly atmosphere during my stay. Especially Winfred MSc., who has supported me throughout my semester project with his patience and knowledge. I am also grateful to Eng. Pedro Salomé, André Sartori and Toze for their assistance on the experimental part of this thesis.

I would like to thank European Union for the financially support and all the staff involved in the EMMS program. Especial thanks to the program coordinator Prof. Margarida Almeida and Prof. Vitor Amaral for their help and concerns on my study. I wish to thank all my friends from University of Aveiro and TUHH, especially Xiaoli, Amit, Andrea and Ram.

I thank my family for their encouragements which helped me to overcome the obstacles in my life.

palavras-chave

Nanocristais de sílicio, films finos, propriedades eléctricas, oxidação, erosão HF

resumo

Filmes finos de nanocristais de sílicio (Si-NCs) depositados sobre substratos flexiveis, usando tintas de sílicio, são atractivos por causa do seu potencial na utilização em dispositivos competitivos em termos de custo e versáteis tais como detectors e dispositivos termoeléctricos. O estudo da preparação e comportamento eléctrico destas redes de nanocristais é fundamental para compreender completamente o seu potencial. Em investigação anterior, filmes de Si-NCs foram depositados por spin coating sobre substratos de polimida e a sua condutividade eléctrica for medida a baixa temperatura e em vácuo.

Neste trabalho, baseado no processo anteriormente desenvolvido, nós estudamos a influência dos diferentes parâmetros de preparação na morfologia e optimizámo-los tais como a concrentação da tinta de Si e a velocidade de rotação durante a preparação por spin coating.

Além disso, investigamos as propriedades eléctricas de filmes de Si-NCs em condições ambientais e à temperatura ambiente, que é considerada uma situação mais realista, no que respeita a aplicações futuras, do que as condições de vácuo e baixa temperatura. Especificamente, o efeito de vários processos fundamentais, tais como tratamento de superfície (erosão HF) dos Si-NCs, dopagem electrónica e iluminação na condutividade eléctrica em condições ambientais foi investigada. Verificamos que as curvas de condutividade versus tempo (σ-t) dos filmes de Si-NCs medidas em condições ambientais apresentam um decaímento rápido causado pela tensão aplicada, seguida pela saturação em valores baixos. Antes do tratamento com HF, nem a exposição à luz nem a dopagem tipo-p leva a uma alteração significativa da condutividade. Depois da remoção dos óxidos nativos dos Si-NCs (tratamento do filmes com HF), um forte efeito da iluminação e da dopagem tipo-p sobre a condutividade é observado, o que indica que a condução nos filmes de Si-NCs é dominada por diferentes mecanismos dependendo de os nanocristais estarem terminados com H ou oxidados. Além disso, da comparação entre medidas eléctricas e ópticas (realizados através de espectroscopia FT-IR), concluimos que a degradação da condutividade dos filmes de Si-NCs tratado com HF que ocorreu por exposição às condições ambientais é essencialmente devida ao crescimento de uma camada de óxido na superfície dos Si-NCs.

keywords Silicon nanocrystals, thin film, electrical properties, oxidation, HF etching

abstract

Thin films of silicon nanocrystals (Si-NCs) deposited onto flexible substrates using silicon inks are attractive because of their potential applications in cost efficient and versatile devices such as detectors and thermoelectric devices. Studying the assembling and electrical behaviour of these nanocrystal networks is fundamental to understand fully their technical potential. In previous research, Si-NC films have been deposited by spin coating process onto polyimide substrates and the electrical conductivity of the resulting films has been measured at low temperature and vacuum conditions.

In this work, based on the previously developed process, we have studied the influence of different assembling parameters on film morphology and optimized the parameters such as the ink concentration and the spin rate for the film fabrication.

Furthermore, we have investigated the electrical properties of Si-NC films at ambient atmosphere and room temperature, which is considered to be a more practical situation with regard to future applications than the vacuum and low temperature conditions. Specifically, the effect of several fundamental processes, such as surface treatment (HF etching) of Si-NCs, electronic doping and illumination on the electrical conductivity at ambient conditions has been investigated. We find that the conductivity-time curves (σ-t) of the Si-NC films measured at ambient conditions show a fast decay caused by the applied voltage, followed by a saturation at lower levels. Before HF etching, neither the light exposure nor the P-doping leads to a significant change of the conductivity. After removal of the native surface oxide layer of Si-NCs (by HF etching of the films), a strong effect of illumination and P-doping on the film conductivity is in turn observed, which indicates that the conduction in Si-NC films is dominated by different mechanisms depending on whether the nanocrystals are H-terminated or surface oxidized. Furthermore, from a comparison between electrical and optical measurements (carried out with FT-IR spectroscopy), we conclude that the degradation of the conductivity of HF-etched Si-NC films that occurred by exposure to ambient conditions is mainly attributed to the growth of the oxide layer on the Si-NC surface.

Table of Contents

List of Figures

List of Tables

Abbreviations

AFM	atomic force microscopy
BET	Brunauer–Emmet–Teller method
EDMR	electrically detected magnetic resonance
EPR	electron paramagnetic resonance
FT-IR	Fourier transform infrared spectroscopy
LB	Langmuir-Blodgett
NLSF	nonlinear least square fitting
PMS	particle mass spectrometer
Rrms	root mean squared roughness
SCLC	space charge limited current
SEM	scanning electron microscopy
Si-dbs	silicon dangling bonds
Si-NCs	silicon nanocrystals
TEM	transmission electron microscopy
VRH	variable range hopping

1 Introduction

1.1 Background and Context

Freestanding semiconductor nanocrystals are aggregates from a few hundreds to tens of thousands of atoms that combine into a crystalline form of matter known as a "cluster" [1]. Their dimensions are typically from a few to tens of nanometers, and those in the sub-ten nanometers size range are often referred to as quantum dots [1]. A strong interest on silicon nanocrystals (Si-NCs) was triggered by the first experimental results demonstrating room temperature luminescence of Si-NCs in silicon-implanted SiO_2 more than twenty years ago [2]. Since then, significant efforts have been devoted to study the unique physical / chemical properties of Si-NCs that are unseen in the bulk form. For instance, while the bandgap of bulk semiconductors is not easily changed, the bandgap of Si nanocrystals can be adjusted in a wide range [3] by the crystal dimensions based on a mechanism known as quantum confinement [4]. Other fundamental properties such as the melting point temperature [5] and hardness [6] can also be changed with the nanocrystal size in comparison to bulk Si. Although the explanations on the size-turnable properties of Si-NCs are still under discussion, extensive research has been engaged to exploit Si-NCs as effective building blocks for the fabrication of entirely new functional devices, such as light emitting display [7], single-electron transistors [8], single-electron memories [9], and hybrid solar cells [10].

In comparison to other nanocrystals of group II-VI and IV-VI compounds, such as cadmium selenide (CdSe) and lead selenide (PbSe), respectively, Si-NCs are of particular interest based on the following reasons. Firstly, many of the II–VI and IV–VI semiconductors contain toxic heavy metals which raise concerns about the environmental issues [11]. Si, at least in the bulk form, is known to be non-toxic and environmentally benign. Secondly, a number of the constituent elements of the II–VI and IV–VI groups face a limited supply in the earth crust and may be unsuitable for large scale applications [11]. On the contrary, availability of Si is hardly a concern since it is the second most abundant element in the earth crust [12]. Prominently, Si-NCs show better compatibility with the well-

established Si-based technology than other candidates, and thus better suitability to scale-up from laboratory processes to industrial applications.

A variety of growth techniques have been developed to produce Si-NCs, such as the thermal segregation of Si-NCs embedded in an oxide matrix [13], laser ablation of a solid state target [14], electrochemical etching of bulk Si [15], colloidal chemistry from solution [16], and the direct formation of nanocrystals in a gas-phase [11]. Controlling the particle size, shape and separations of the Si-NCs requires sophisticated techniques by adjusting concerning process parameters. To achieve a large-scale output of Si-NCs for the production of functional raw materials, the colloidal chemistry and the gas-phase route seem to be scalable to an industrial level.

Due to their small sizes, Si-NCs can be converted into printable inks, processed with many of the inexpensive techniques that for example make organic materials attractive, yet they are expected to have superior mobility and resistance to degradation. Typically, the Si inks can be applied to print thin films of functional materials in the form of three-dimensional networks [17], [18]. The bottom-up assembling of Si-NC films via printing-type methods such as drop casting, spin-coating or inkjet printing can improve the flexibility and reduce the fabrication cost tremendously. Moreover, printing has also the advantage of separation of the high temperature synthesis of nanocrystal growth and the deposition steps. Therefore, substrates with low melting temperature such as flexible polymers can be applied for film deposition. Recent studies have shown that thin films of Si-NCs processed from Si inks present interesting optoelectronic properties [19] and thermoelectric effects [20], which might be exploited respectively for the development of photo-detectors and thermoelectric devices. This new type of functional layers (deposited onto flexible substrate) might expand the application range of these devices from Si into new areas where cost-effective, versatile and low temperature fabrication is required.

1.2 Scope, Objectives and Overview

Within the above context, studying the assembling and the electrical behaviour of thin films of Si-NCs is one of the critical and fundamental steps to exploit their technological potential. However, the film morphology and its macroscopic electrical behaviour have not

been fully understood yet, mainly attributed to the difficulties in preparation of high-quality Si-NCs. In previous research, Si-NC films were deposited onto flexible polyimide (Kapton®) substrates by a spin coating process using dispersed Si inks (a mixture of Si-NCs and ethanol). The temperature dependent conductivity changes of the resulting films were measured from about room temperature to 100 K in a vacuum environment [18]. Based on the previously developed process, we will study in this work the dependence of the film morphology on different process parameters to gain further understanding regarding the assembling of Si-NCs. Moreover, we will investigate the electrical properties of Si-NCs films at ambient atmosphere and room temperature which are more relevant for the practical situation of future applications than the vacuum and low temperature conditions. Specifically, the electrical conductivity at ambient conditions will be studied with regard to the effects of the surface treatment (HF etching of Si-NCs), the electronic doping, the dispersion method of Si inks, and illumination. Besides, to have a further understanding on the electrical behaviour of our Si-NC films, we will study the surface state of Si-NCs by applying FT-IR spectroscopy.

This thesis is organized as follows. Firstly, a review is given concerning the application of wet techniques for assembling Si-NCs into thin films and current knowledge about the electrical characteristics of Si-NC films. Next, we will focus on experimental aspects, including the film preparation and a description of characterization techniques applied in this work. The experimental results will be then discussed in detail, in terms of the film morphology, the electrical measurements and the characterization of the surface state of Si-NCs. The conclusions and the outlook for future work are summarized in the last chapter.

1.3 References

[1] Retrieved from http://www.nanodic.com/nanomaterial/Nanocrystal.htm, (2009).

[2] S. Furukawa and T. Muyasat, J. Appl. Phys. Part 2 L2207 (1988) 27.

[3] X.D. Pi, R.W. Liptak, J.D. Nowak, et al., Nanotechnology 19 (2008) 24.

[4] A.P. Alivisatos, Science 271 (1996) 4.

[5] Z. Zhang, M. Zhao, and Q. Jiang, Semicond. Sci. Technol 6 (2001) 2.

[6] W.W. Gerbericha, W.M. Mook, C.R. Perrey, et al., J. Mech. Phys. Sol. 51 (2003) 979.

[7] K. Nishiguchi, X. Zhao, and S. Oda, J. Appl. Phys. 92 (2002) 2748.

[8] S. Tiwari, H. Hanafi, A. Hartstein, et al., Appl. Phys. Lett. 68 (1996) 1377.

[9] Y.T. Tan, T. Kamiya, Z.A.K. Durrani, et. al, J. Appl. Phys. 94 (2003) 633.

[10] C.Y. Liu, Z.C. Holman, and U.R. Kortshagen, Nano Lett. 9 (2009) 52.

[11] U.R. Kortshagen, J. Phys. D: Appl. Phys. 42 (2009) 113001.

[12] G..B. Haxel, J.B. Hedrick, and U.S. Orris, U.S. Geological Survey (2002).

[13] M. Fujii, Y. Inoue, S. Hayashi, et al., Appl. Phys. Lett. 68 (1996) 26.

[14] T.A. Burr, A.A. Seraphin, E. Werwa, et al., Phy. Rev. B 56 (1997) 8.

[15] D. Nielsen, L. Abuhassan, M. Alchihabi, et al., J. Appl. Phys. 101 (2007) 114302.

[16] J. Zou, P. Sanelle, K.A. Pettigrew, et al., J. Cluster Sci. 17, (2006) 565.

[17] R. Lechner, A.R. Stegner, R.N. Pereira, et al., J. Appl. Phys.104 (2008) 053701.

[18] A.R. Stegner, R.N. Pereira, K. Klein, et al., Phys. Rev. Lett. 100 (2008) 026803.

[19] S. Pradhan, S.W. Chen, J. Zou, et al., J. Phys. Chem. C 112 (2008) 13292.

[20] R. Lechner, H. Wiggers, A. Ebbers, et al., Phys. Stat. Sol. 6 (2007) 262.

2 State-of-The-Art

2.1 Assembly of Si-NC Films

Freestanding nanocrystals provide means to define precisely a nano-scale device using 'bottom-up' fabrication routes rather than conventional fabrication methods, such as lithography and etching on bulk materials [1]. This new approach to fabricate nano-scaled silicon structures is of particular research interest in the field of Si electronics, where the conventional top-down miniaturization trend is getting exceedingly hard due to fundamental physical and technological limitations as well as economical limitations [2]. Moreover, as mentioned in the previous chapter, the development of new technology for assembly of nanocrystals provides us with an enormous improvement of flexibility in device design and fabrication. The use of wet techniques in the field of colloidal particle science is one of the promising approaches for nanocrystal assembling, which might be suitable to scale-up to an industrial level because they are cost efficient and easy for manipulation. Since we also applied a wet approach for the fabrication of Si-NC films, in this section, we will introduce the application of similar techniques in the formation of two dimensional array or films of Si-NCs. The morphology of the corresponding assembling will also be discussed.

An approach which is quite relevant to this work can be seen in reference [3]. Spherical Si-NCs produced from gas phase were dispersed in ethanol by using a ball milling process. Then the Si-NC dispersions were spin coated onto flexible Kapton substrates, resulting in porous layers of Si-NCs (porosity of 60-70%) with a thickness of several hundreds nanometers. Lechner et al. [4] used a laser annealing process to sinter the layer of Si-NCs, resulting in melting and recrystallization of the particles. However, they found that the overall morphology after laser annealing can still be described as a porous film. The estimated porosity is roughly the same as before the annealing, with only the pore sizes and structure dimensions having increased significantly. An example of the film morphology after laser annealing process is shown in Fig. 2.1.

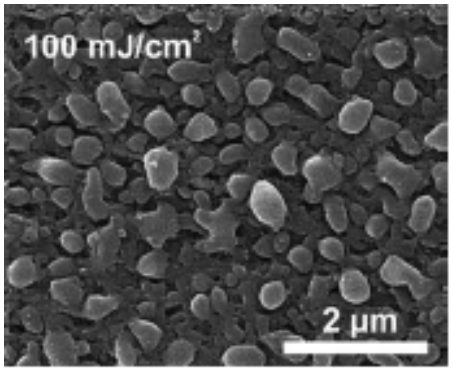

Fig. 2.1 The spin coated Si-NC films after laser annealing at the indicated energy densities. The radius of Si-NCs before laser annealing is 20 nm [4].

Tanaka et al.[2] have developed a method of assembling the Si-NCs from the solution by using a drop and evaporation technique (or drop casting). The Si-NCs with a diameter of 8±1nm were deposited on the Si substrates by using plasma enhanced decomposition of SiH_4 gas. The resulting deposition on the Si substrate were then immersed into a solvent and applied ultrasonic treatment to remove Si-NCs from the substrate surface and disperse them into the methanol solvent. A flow chart is given in Fig. 2.2 to illustrate the process. A drop of dispersed solution was then taken onto a hydrophilic SiO_2 substrate and evaporated at room temperature to form the two dimensional array of Si-NCs. Figure 2.3 shows a scanning electron morphology of the resulting array. The array is found to be a monolayer of Si-NCs with lots of voids. The areal dot density is estimated to be about 5×10^{11} dots/cm^2. The physics behind this method is to form contact between the Si-NCs during the liquid evaporation by using the lateral capillary meniscus force [5]. Further experiments were performed by making the evaporation process slower at -40 ℃ with use of isopropanol as a solvent. They found that by doing so the areal dot density of the layer increases to 9.4×10^{11} dots/cm^2.

Fig. 2.2 A schematic flow–chart of the drop and evaporation process [2].

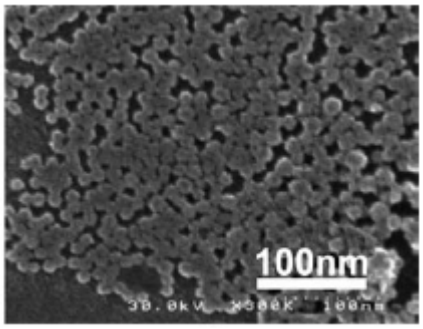

Fig. 2.3 A SEM image of Si-NCs assembled by the drop and evaporation process using methanol solvent on SiO_2 substrate [2].

In a recent study [6], the Langmuir-Blodgett (LB) technique has been applied to fabricate a two dimensional assembly of Si-NCs. The Si-NCs (10±1 nm) were produced in an ultra high vacuum (UHV) chamber using VHF plasma decomposition of a pulsed SiH_4 gas supply. In comparison to the drop casting method discussed above, the LB technique is a more controllable method with molecular level precision, which was originally used for fabrication of two dimensional structures of organic molecules [7].

The overall procedure of producing a mono-layer of Si-NCs can be generally described by the following four steps.

(1) Surface treatment of Si-NCs. The as-deposited Si-NCs react with pure water and easily go down into water. Hexamethyldisilazane (HMDS), a silane coupling agent, was used to coat the nanocrystal surface so that the surface becomes hydrophobic.

(2) Preparation of Si-NC suspension. The surface treated Si-NCs are then dispersed into chloroform solvent resulting in a suspension.

(3) Drop of the suspension on water. The suspension spread along the air-water interface of a Langmuir trough, and the Si-NCs covered by HMDS float on pure water because of surface tension.

(4) Transfer the film to a solid substrate. This step is conventionally done in the LB technique by compression of the floated mono layer laterally onto a immersed substrate

The resulting films of HMDS coated Si-NCs (diameter ~10 nm) have a lattice like structure, as shown in Fig. 2.4. The Si-NCs are homogenously distributed in the film and densely packed. The areal density is estimated to be 7.33×10^{11} dots/cm^2.

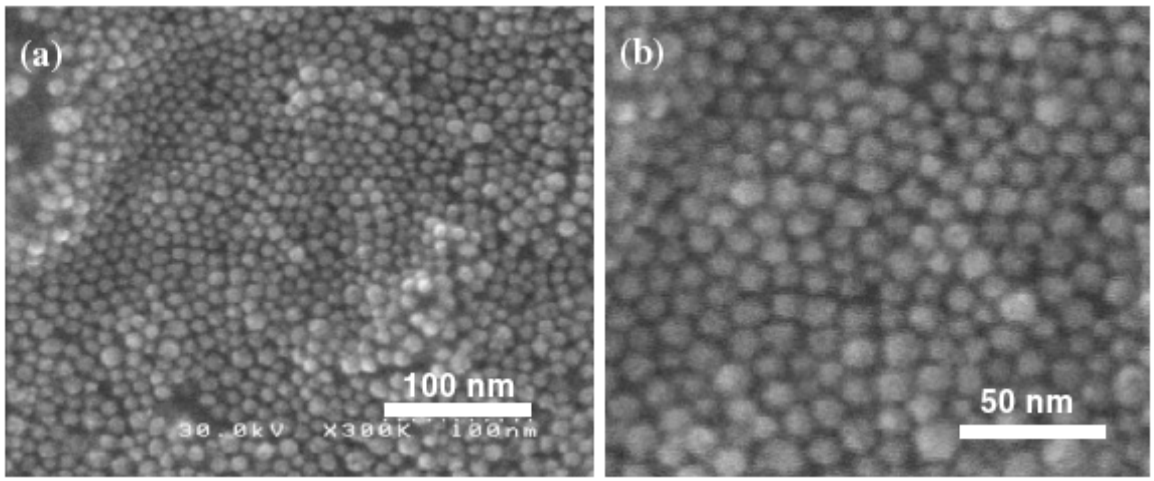

Fig. 2.4 SEM images of an LB film of HMDS-coated Si-NCs [6].

2.2 Electrical Conduction in Si-NC films

At present, there are only limited investigations on the macroscopic electrical characteristics of Si-NC films. Among them, the temperature-dependent conductivity of Si-NC films is most intensely studied by different research groups [8-12]. The electrical behaviour for example I-V curve changes with the temperature, and have been explained by different conduction mechanisms, such as space charge limited current (SCLC) [13] and thermally activated tunnelling [14]. Moreover, a development on the electronic doping technique has

triggered the investigation of the electrical behaviour of films constituted by doped Si-NCs [3, 4]. A recent study on the photoconductivity of LB monolayer of Si-NCs [11] is also introduced additionally.

2.2.1 Temperature-Dependent Conductivity

Rafiq et al. have investigated the I–V characteristics as the temperature varies from 300 K to 30 K [8, 9]. The I–V measurements were performed using Al/Si-NCs film/ p-Si/Al 'mesa' structures, where current flow was vertically across the film (Fig. 2.5a). The films were prepared using plasma decomposition of SiH_4. The Si-NCs are undoped, ~ 8 nm in diameter with a thin (around 1–2 nm) surface SiO_2 layer (Fig. 2.5b and c). They have found that I-V curve shows a power law dependence ($I \sim V^m$) from 300 to 200 K (with m increase from 1.8 to 4). However, below 200 K, such a feature is not presented. Instead, a constant m is obtained. Moreover, an Arrhenius plot of conductivity as a function of temperature shows two distinct regimes (Fig. 2.6). Above 200 K (black circles), a single, steep slope is observed, while below 200 K, the data (white circles) can be fitted to a $\ln(\sigma)$ vs $T^{1/2}$dependence. Similar result has also been reported by Lau et al. with the Si-NCs film prepared from solid state reactions [10] and by Pradhan et al. with LB monolayer of Si-NCs [11] .

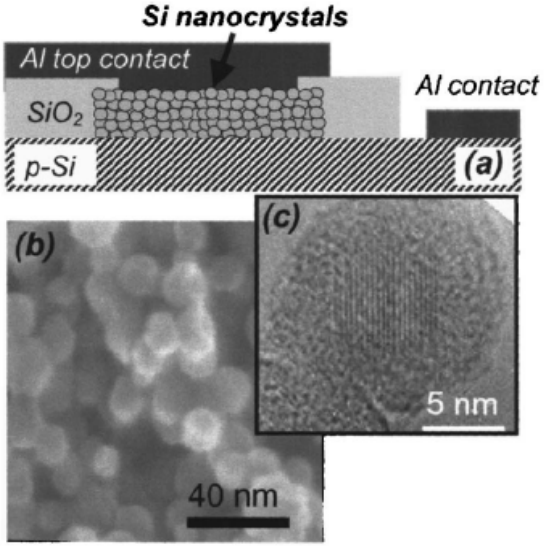

Fig. 2.5 (a) Schematic of the Al/Si-NCs/ p-Si/Al diode; (b) Scanning electron micrograph of the Si-NCs film; (c) Transmission electron micrograph of a Si-NC [8].

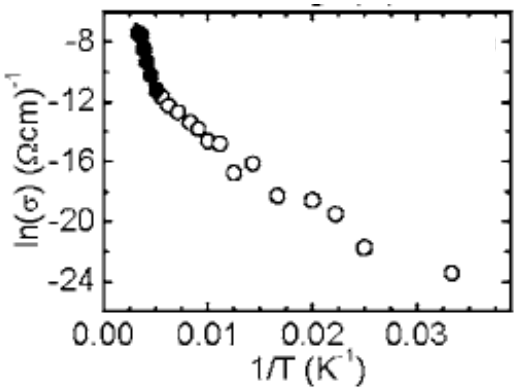

Fig. 2.6 Arrhenius plot of conductivity σ as a function of temperature T, at 4V bias across the film [8].

The power law dependence $I \sim V^m$ at high temperature range can be explained by the SCLC model with an exponential distribution of carrier traps [8], [13], whereas the ln(σ) *vs* $T^{1/2}$dependence at lower temperature range is associated with the tunnelling model of thermally activated carriers between neighbouring NCs [9], [14]. Besides, variable range hopping (VRH) mechanisms, such as the Efros-Shklovskii VRH [15] and the Mott VRH [16], are also suggested to explain the ln(σ) *vs* T^n ($1/4 \leq n \leq 1/2$) dependence [17]. The hopping is considered to occur not only in the transport band of Si-NCs, but also involved the defects states [9], [18], which further complicate the analysis.

The macroscopic conduction of Si-NC films observed from different research groups are somehow different, resulting in debates over the electronic transport mechanisms. For example, some researchers observe no significant influence of the temperature on the conductivity below 100 K and slight temperature dependence above this temperature, which was further interpreted by temperature-independent geometrical effects and low temperature-dependent electronic effects, respectively [12]. The different observation might be due to different assembling of Si-NCs regarding for example the nanocrystal size, the surface state of Si-NCs and the density of the films. The measurement methods like the electrode contacts can also affect the results. For example, Burr et al. have shown the I-V curve in thin films of Si-NCs changes depending on the electrode construction [12].

2.2.2 Influence of Doping

Doping is an effective method to improve the electrical conductivity of semiconductors. However, the doping of semiconductor nanocrystals is quite different from the

corresponding bulk materials. For example, the electron concentration of the doped nanocrystals at room temperature can be reduced by effects such as the self-purification and the increase of the donor ionization energy [19], [20]. Moreover, due to their very large surface-to-volume ratio, surface termination is also expected to have a strong influence on the doping of nanocrystals and the electronic properties [18]. The future application of Si-NC films requires a sophisticated electronic doping method for Si-NCs, and a good understanding about the influence of doping on the electrical properties of the films.

It has been reported recently that both n- and p-type doping can be achieved in Si-NCs produced in microwave plasma from the gas phase, by adding the dopant sources to the precursors [21]. The doping level can be controlled by changing the concentration of the dopant sources. Lechner et al. [4] have investigated the conductivity of the films made of doped Si-NCs produced by this technique. They found that the doping concentration can be varied over a wide range and the conductivity is adjustable once a critical doping concentration is exceeded. Figure 2.7 shows the conductivity changes of the Si-NC films in relation to the doping concentration. Note the laser annealing is applied in this study to improve lateral conductivity of the Si-NC film as a result of the sintering and melting of the particles. The critical doping concentration is suggested to be determined by the defect concentration, which compensates the charge carriers and most likely results from the dispersion method.

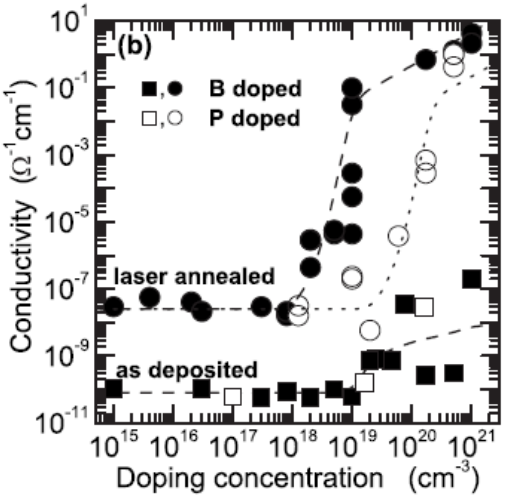

Fig. 2.7 Electrical conductivity of B- and P-doped layers of Si-NCs before and after laser annealing as a function of the doping concentration. The lines are guides for the eyes. The dotted line corresponds to the dashed line shifted to higher doping concentrations by a factor of 20 [4].

The temperature-dependent conductivity changes of the doped Si-NC films have also been studied with respect to the doping concentration [3]. It is found that doping of Si-NCs strongly influences the conductivity of the films. As shown in Fig. 2.8, an increase of the Si-NCs doping concentration results in an increase of the films conductivity and in a decrease of the temperature dependence of the conductivity [3]. Further electrically detected magnetic resonance (EDMR) and electron paramagnetic resonance (EPR) measurements demonstrated that a direct participation of P donor and Si dangling bonds (denoted as Si-dbs) states in the electronic transport through Si-NC networks: P donors and Si-dbs contribute to dark conductivity via spin-dependent hopping, whereas in photoconductivity, these states are shown to act as recombination centres of excess charge carriers [3, 18].

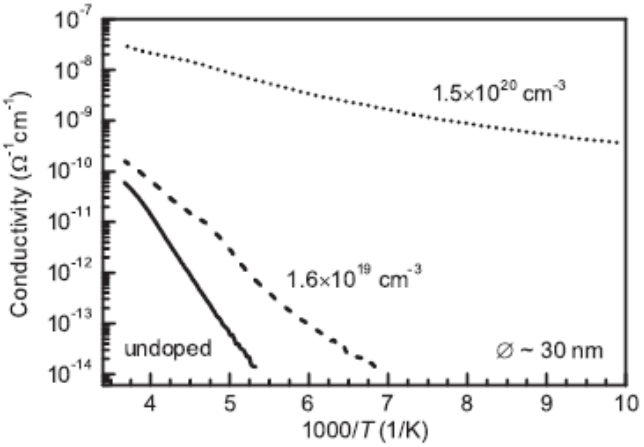

Fig. 2.8 Arrhenius plot of dark conductivity as a function of temperature for films of Si-NCs (diameter ~30 nm) doped at different levels, measured with an applied voltage of 20 V and after removal native oxide by HF etching [3].

2.2.3 Photoconductivity

Pradhan et al. [11] have studied the photoconductivity of LB monolayers of Si-NCs (core diameter 3.86± 0.85 nm) in vacuum and at controlled temperature. The Si-NCs were coated with a siloxane-structure by a silanization process to enhance their surface stability [11], [22]. Figure 2.9 summarizes the variation of the conductivity of the LB monolayer at different temperature in the dark and in the presence of photoirradiation by four different lasers: UV (355 nm), blue (473 nm), green (532 nm), and red (638 nm).

Firstly, it can be seen that at any temperature, the higher the photon energy, the greater the enhancement of the conductivity, i.e., dark ≈ red < green < blue < UV. Here, the absorption threshold (corresponds to the critical absorption bandgap) is at the green laser wavelength position (532nm). Typically, at room temperature, the photoconductivity is 0.13 mS/m (illuminated by blue laser) and 0.19 mS/m (illuminated by UV laser), which is about 1.7 and 2.5 times higher than the conductivity measured at dark condition (0.075 mS/cm), respectively.

Secondly, in the dark or the condition of lower photon energy (red light), the conductivity increases drastically with temperature, which was attributed to the conduction of thermally activated charge carriers. In contrast, at higher photo energy (green, blue and UV light), the photoconductivity becomes virtually independent of temperature, suggesting that the photo-excited free carriers, which are efficiently ionized from photo generated electron-hole pairs by the applied electrical field, are dominant in electrical conduction.

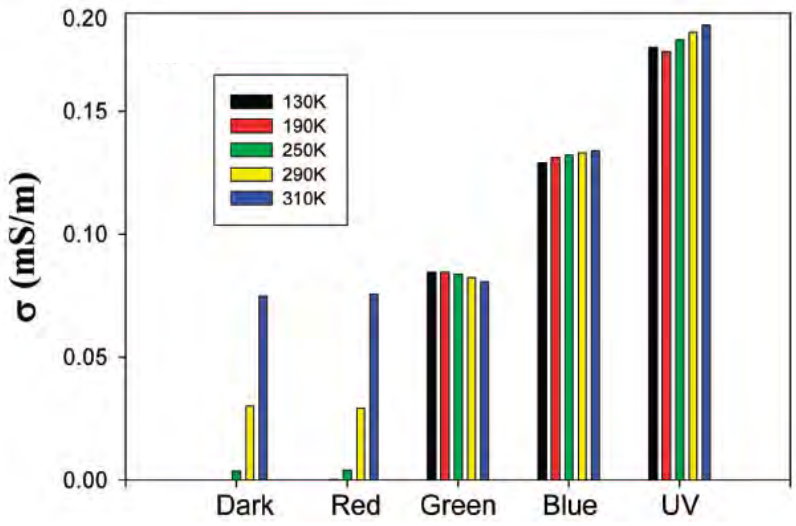

Fig. 2.9 Conductivity of LB monolayers of Silicon nanoparticles at different temperature in the absence (dark) and presence of photoirradiation by four different lasers [11].

1 mS/m = 10^{-5} $\Omega^{-1}cm^{-1}$

2.3 References

[1] Z.A.K., A.B. Durrani, and M.A. Rafiq, Microelectro. Eng. 86 (2009) 456.

[2] A. Tanaka, Y. Tsuchiya, K. Usami, et al., Curr. App. Phys. 6 (2006) 344.

[3] A.R. Stegner, R.N. Pereira, K. Klein, et al., Phys. Rev. Lett. 100 (2008) 026803.

[4] R. Lechner, A.R. Stegner, R.N. Pereira, et al., J. Appl. Phys.104 (2008) 053701.

[5] P.A. Kralchevsky, S.W. Chen, J. Zou, et al., J. Phys. Chem. C 112 (2008) 13292.

[6] A. Tanaka, Y. Tsuchiya, K. Usami, et al., Jpn. J. Appl. Phys. 5 (2008) 47.

[7] M. Murata, M. Villeneuve, H. Nakahara, et al., Chem. Phys. Lett. 405 (2005) 416.

[8] M.A. Rafiq, Y. Tsuchiya, H. Mizuta, et al., Appl. Phys. Lett. 87 (2005) 182101.

[9] M.A. Rafiq, Y. Tsuchiya, H. Mizuta, et al., J. Appl. Phys. 100 (2006) 14303.

[10] H.W. Lau, O.K. Tan, and D.A. Trigg, Appl. Phys. Lett. 89 (2006) 113119.

[11] S. Pradhan, S.W. Chen, J. Zou, et al., J. Phys. Chem. C 112 (2008) 13292.

[12] T.A. Burr, A.A. Seraphin, E. Werwa, et al., Phy. Rev. B 56 (1997) 8.

[13] M.A. Lampert and P. Mark, Current Injection in Solids Academic, New York, (1970).

[14] M. Fujii, O. Mamezaki, S. Hayashi, et al., J. Appl. Phys. 83 (1998) 1507.

[15] A.L. Efros and B.I. Shklovskii, J. Phys. C 8 (1975) 49.

[16] N.F. Mott, Philos. Mag. 19, (1969) 835.

[17] M. Fujii, Y. Inoue, S. Hayashi, et al., Appl. Phys. Lett. 68 (1996) 26.

[18] R.N. Pereira, A.R. Stegnera, K. Klein, et al., Physica B 401-402 (2007) 527.

[19] G.. Cantele, E. Degoli, E. Luppi, et al., Phys. Rev. B 72 (2005) 113303.

[20] G..M. Dalpian and J.R. Chelikowsky, Phys. Rev. Lett. 96 (2006) 226802.

[21] B. Giesen, H. Wiggers, A. Kowalik et al., J. Nanopart. Res. 7 (2005), 29.

[22] J. Zou, R.K. Baldwin, S.M. Kauzlarich, et al., Nano Lett. 4 (2004) 7.

3 Experimental Work

3.1 Preparation of Si-NC films

In this work, Si-NCs are grown from a gas-phase and dispersed in ethanol, resulting in a Si-NC suspension (so-called Si ink). An ultrasonication approach is applied to disperse the Si ink, apart from the previously used ball milling process [1], [2]. Afterwards, the resulting Si ink is spin coated onto a piece of polyimide substrate (Kapton®) to form a thin film of stacked Si-NCs.

3.1.1 Growth of Silicon Nanocrystals

The Si-NCs are prepared by microwave-induced decomposition of silane in a low-pressure microwave plasma reactor. The experimental setup is schematically depicted in Fig. 3.1 [3]. The reactor consists mainly of a quartz glass tube into which the premixed reaction and dilution gases (SiH_4, H_2, and Ar) are injected. The microwave energy is coupled into the gas flow forming a flame-like plasma torch, which leads to the dissociation of the silane precursor. The generated particles are separated from the exhaust gases in the extraction chamber and collected on a surface. In some cases, the particle size can be measured in situ using a particle mass spectrometer (PMS). In the case of the Si-NCs used in this study, the mean particle size was determined by means of the Brunauer–Emmet–Teller method (BET, [4]).

Figure 3.2 shows the TEM images of the Si-NCs produced by this method. As can be seen, the Si-NCs are spherical and show a crystalline core and an amorphous oxide layer on the surface (Fig. 3.2b), which is formed after exposure to ambient air [3]. The mean particle size can be adjusted by varying the precursor concentration, the pressure and the microwave power [3]. It is reported that the Si-NCs follow a log-normal size distribution with a deviation of the diameter of σ = 1.3-1.5. Both phosphorus and boron doping can be achieved by using phosphine (PH_3) and di-boran (B_2H_6) as additional precursor material, respectively [5].

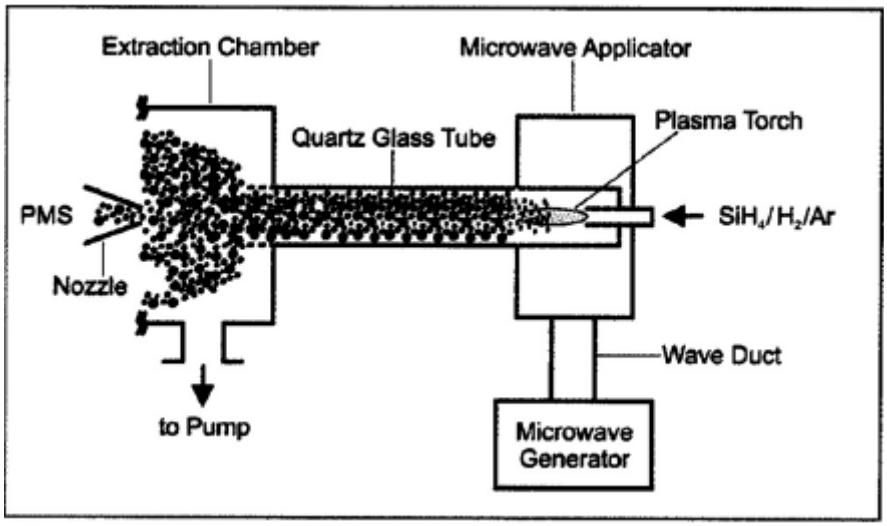

Fig. 3.1 Microwave plasma system for the synthesis of semiconductor nanocrystals [3].
The main components are (in downstream sequence): Gas inlet, microwave system consisting of the microwave generator, the wave duct and the microwave applicator, quartz glass tube, particle extraction chamber with a particle mass spectrometer (PMS) and a pumping system.

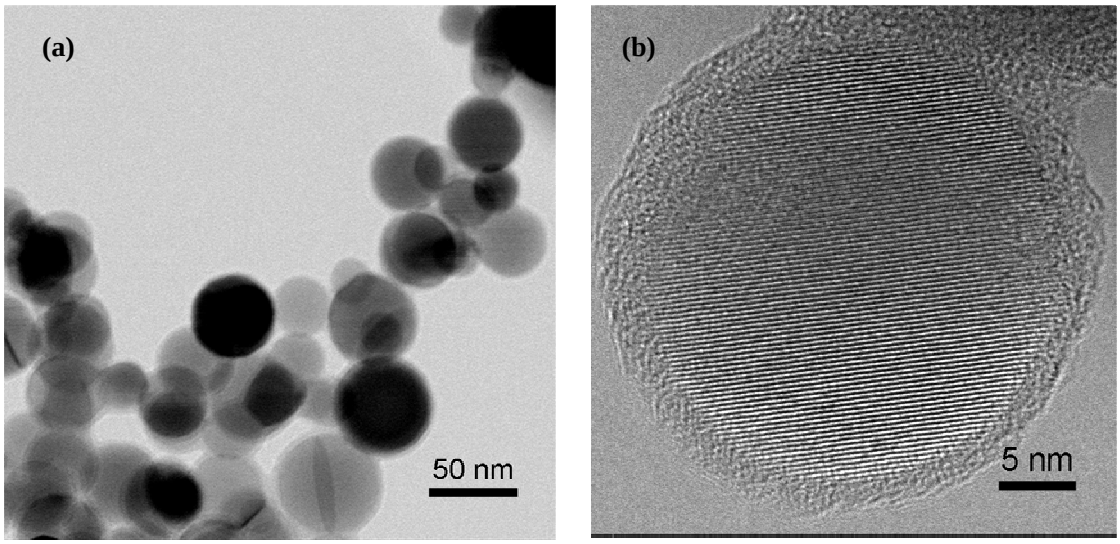

Fig. 3.2 The spherical Si-NCs produced from the microwave plasma reactor.
(TEM Images obtained at the University of Aveiro).
(a) Spherical Si-NCs. (b) A Si-NC with a crystalline core and surface of amorphous oxide.

There are two types of Si-NCs used in this work, which were fabricated at the *Institut für Verbrennung und Gasdynamik* at University of Duisburg-Essen in Germany, with basic properties summarized in Tab. 3.1. The nominal doping concentration is defined as the

fraction of the flow of the dopant source (PH_3) in the total amount of precursor gases multiplied by the atomic density of silicon.

Tab. 3.1 Parameters of Si-NCs used in this work

Label of the Si-NCs	Type	Doping concentration	Average particle size
140906	Intrinsic	N/A	46.8 nm
050608	P-doped	5×10^{20} /cm^3	45.0 nm

3.1.2 Nanocrystal Dispersion

A standard ball milling process has been used in previous research to disperse Si-NCs into Si inks [1], [2]. In this work, the Si ink (5 wt.% of Si-NCs in ethanol) was ball milled with yttrium stabilized ZrO_2 beads for 4.5 hours in a thermomixer compact. An IKA® Mixing/Shaker was used for this process with an orbital rotation speed of 2500 rpm.

It has been reported recently that the ball milling process causes a strong increase of the density of Si-dbs [2], which can lead to compensation of charge carriers and thus degradation of electrical performance. The ultrasonic energy is known to be an effective tool to disperse nanomaterials [6]. Therefore, we have prepared Si-NC films from ultrasonic dispersed Si inks, and these films were compared with the films produced from the ball milled Si inks regarding their film morphology and electrical properties. The ultrasonic dispersion was done with an ultrasonic bath (Bandelin Sonorex®, RK255H, power 300 w, frequency 40 KHZ) and the dispersion time is ~ 4.5 hours.

3.1.3 Spin coating

Spin coating involves the acceleration of a liquid puddle on a rotating substrate and evaporation of the liquid substance. To produce Si-NC films, a drop of the Si ink was deposited in the centre of a Kapton substrate immediately after the dispersion process. The Si-NCs stacks to form a film once the ethanol is evaporated during the substrate spinning. A Spincoater® (Speedline Technologies, model P6708) was used for this process.

3.1.4 Removal of the native oxide

A surface oxide layer is formed on the as-grown Si-NCs after they are exposed to ambient air [3]. This oxide layer remains as a barrier that impedes the movement of electrical carriers between Si-NCs. To remove the native oxide, the surface of the Si-NCs in the films was etched in a dilute HF acid solution (5 vol.% in H_2O). A Teflon® rod was used to hold the Kapton substrate and dip the Si-NC film into the HF acid. After 10 second etching, a gentle blow of compressed air is applied to dry the sample.

3.2 Experimental Characterization Methods

In this section, the basic principles of the technologies used to characterize our Si-NC films are introduced in brief, including thickness profilometer, scanning electron microscopy (SEM), atomic force microscopy (AFM), conductivity measurement and FT-IR spectroscopy. The parameters of the experimental setups are also presented.

3.2.1 Film Thickness: Dektak Profilometer

The Dektak profilometer is operated by lightly dragging a sharp stylus over the surface of the substrate and recording the vertical profile of the surface. It provides a quantifiable measurement of the surface profile of a substrate, like wafers and thin films. It can be used to measure the height or width of a feature on the surface. The profile recorded can also give a look at the roughness of the measured surface [7].

The thickness of our Si-NC films was measured using a Dektak profilometer (Veeco® 150). The basic setup parameters can be found in Tab. 3.2.

Tab. 3.2 Parameters of thickness measurement carried out with Dektak profilometer

Stylus Radius	Scanning duration	Resolution	Force	Measurement Range
12.5 µm	30 sec.	0.167 µm	1.00 mg	6.5 µm

3.2.2 Film Morphology: SEM and AFM

The SEM is a type of electron microscopy that provides images of a sample surface by scanning it with a high-energy beam of electrons. The electrons interact with the atoms at or close to the sample surface producing signals including secondary electrons (SE), back-scattered electrons (BSE), characteristic X-rays, auger electrons and etc. In the most common or standard detection mode, SE imaging can produce very high-resolution images of a sample surface, revealing topographical details in nanometer scales, whereas BSE are used to provide information about the distribution of different chemical elements in the sample [8]. In this study, the SEM (Hitachi, model SU-70) is applied in the SE detection model to characterize the morphology of our Si-NC films.

The AFM is a type of high resolution scanning probe microscopy. It consists of a cantilever with a sharp tip (probe) which is used to scan the specimen surface. When the tip is brought into proximity of a sample surface, forces between the tip and the sample lead to a deflection of the cantilever according to Hooke's law. In most cases a feedback mechanism is employed to adjust the tip-to-sample distance to maintain a constant force between the tip and the sample. It is this adjustment that is displayed as data, resulting in a map of the scanning areas which represents the topography of the sample. In general, the imaging modes are divided into static (or contact) modes and a variety of dynamic (or non-contact) modes depending on the applications. Unlike the SEM which only provides a two-dimensional image of a sample, the AFM provides a true three-dimensional surface profile. Additionally, samples viewed by AFM do not need any coating treatment to increase surface conduction which would irreversibly change or damage the sample [9].

As an addition to the SEM characterization, in this work, the AFM (NanoScope® IIIa,Veeco Metrology Group) is applied in a contact model to reveal the surface roughness of the films and to have a three dimensional impression of the Si-NC assembling. Silicon SPM sensor (Pointprobe®) was used with Pt/Ir coating on the tip side and with a force constant at 2.8 N/m.

3.2.3 Electrical Conductivity

3.2.3.1 Preparation of the metal contacts

In order to characterize the electrical properties of Si-NC films, the films were deposited onto a flexible polyimide (Kapton®) substrate, where interdigit gold contacts have been deposited previously. Designed for conductivity measurement, the gold grids consist of 112 digits of 10 μm widths and 10 μm spacing. They are fabricated by the lift-off process, as illustrated schematically in Fig. 3.3. Firstly, a photoresist is deposited on the Kapton by spin coating and patterned by the photolithography process (exposing and development). A gold layer is then evaporated thermally all over the substrate, covering the photoresist and areas in which the photoresist has been cleared. Afterwards, the photoresist under the gold layer is removed with acetone, taking the gold with it, and leaving only the gold grids which were deposited directly on the substrate. The resulting structure can be seen in Fig. 3.4.

3.2.3.2 Measurement principle

The electrical measurements were carried out in dark and at ambient atmosphere by a two-point method. During the measurement, a constant DC voltage (for example, 80 V) is applied for some time from a few minutes to several hours and the current changes are monitored, resulting in a current-time (I-t) curve from which the corresponding conductivity-time (σ-t) curve can be calculated based on the following equation.

$$\sigma = \frac{I \cdot d}{n \cdot U \cdot T \cdot l} \qquad \text{Eq. 3.1}$$

where σ is the conductivity, I the current, d the distance between each digit (10 μm), n the number of digits (112), U the applied DC bias, T the film thickness and l the length of the digit (2 mm). For carrying out electrical measurement under photo-excitation (photoconductivity), a halogen lamp with a power density of 100 W/cm^2 was used as a light source. The voltage that can be applied for conductivity measurements is in the range of 0-80 V.

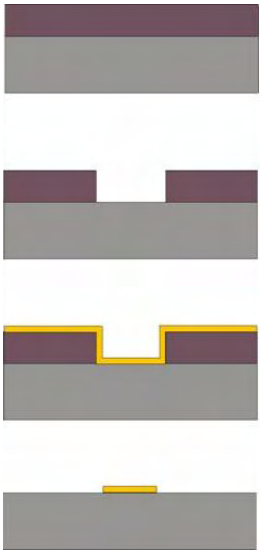

a) substrate with deposited photoresist

b) Following expose and development

c) Gold evaporation

d) Removal by acetone, lift-off

Fig. 3.3 Procedure of the lift-off process to fabricate gold grids on the Kapton substrate.

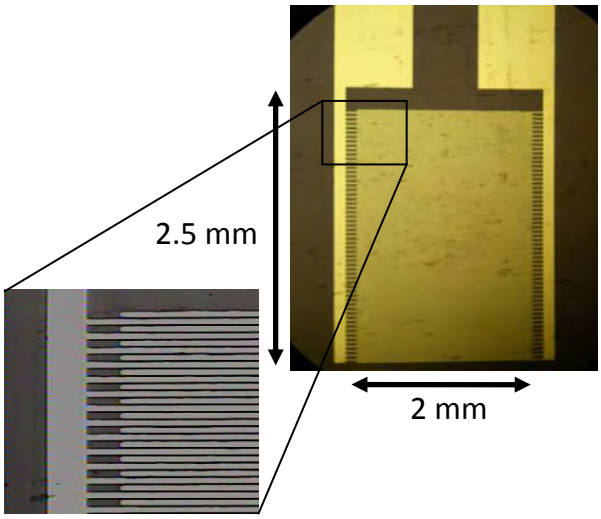

Fig. 3.4 Gold contacts on the Kapton substrate.

3.2.4 FT-IR

FT-IR spectroscopy is a chemically specific analysis technique, which provides information about the chemical bonding or molecular structure of materials [10]. During the measurement, a spot on the sample is subjected to a modulated IR beam. The transmittance and reflectance of the infrared rays at different frequencies is translated into an IR spectrum consisting of various bands and peaks. The "translation" procedure is facilitated by using a Fourier transform instrument which can measure all wavelengths simultaneously.

The resulting infrared spectrum represents a fingerprint of a sample with absorption peaks which correspond to the frequencies of vibrations of the bonds between the atoms. Analysis of these absorption characteristics reveals details about the molecular structure of the sample. In addition, the size of the peaks in the spectrum is a direct indication of the amount of material present.

Infrared spectroscopy can be used as a reliable technique to characterize the structure, chemistry and reaction dynamics on the surface of Si materials. For example, by measuring at a specific frequency over time, changes in the character or quantity of a particular bond (e.g. Si-O-Si on the bulk Si surface [11]) can be measured, which provides prompt and accurate information regarding chemical reactions occurred on the sample surface.

In this study, the surface state of the Si-NCs in the films was studied by FT-IR spectroscopy. The measurements were carried out with an evacuated Bruker IFS 66v spectrometer. Other parameters can be found in Tab. 3.3.

Tab. 3.3 Parameters of the FT-IR spectroscopy

Source setting	Aperture size	Beam splitter	Scanning velocity	Resolution
Mid-wave infrared	2.5 mm	KBr	60 KHZ	2 cm^{-1}

3.3 References

[1] R. Lechner, A.R. Stegner, R.N. Pereira,et al., J. Appl. Phys.104 (2008) 053701.

[2] R.N. Pereira, A.R. Stegnera, K. Klein, et al., Physica B 401-402 (2007) 527.

[3] J. Knipping, H. Wiggers, B. Rellinghaus, et al., J. Nanosci. Nanotech. 4 (2004) 1039.

[4] S. Brunauer, P. Emmet, and E. Teller, J. Amer. Chem. Soc. 60 (1938) 309.

[5] B. Giesen, H. Wiggers, A. Kowalik et al., J. Nanopart. Res. 7 (2005), 29.

[6] S.J. Chung, J.P. Leonard, I. Nettleship, et al., Powder Tech. 194 (2009) 75–80.

[7] J. Frensley, Document FA2003-TF-001, Univ. Texas at Dallas (2003).

[8] Retrieved from http://en.wikipedia.org/wiki/Scanning_electron_microscope (2009).

[9] Retrieved from http://en.wikipedia.org/wiki/Atomic_force_microscope (2009).

[10] Document from Thermal Nicolet Corporation, Introduction to FT-IR (2001).

[11] M. Niwano, J. Kageyama, K. Kurita, et al., J. Appt. Phys. 76 (1994) 2157.

4 Film Morphology

Studying the morphology of Si-NC films provides a direct approach to select appropriate processes and processing parameters to produce films with adequate properties. Moreover, it is helpful to understand the macroscopic properties of the films, like the electrical conductivity. This chapter presents a discussion on the film morphology concerning various aspects, which are organized as the following. Firstly, the film thickness is studied as a function of the spin rate and the ink concentration (weight percentage of Si-NCs in the ink). Besides, the influence of the ink concentration and the dispersion methods on the surface morphology is investigated. Further comparison will be made between the film morphology observed before and after HF etching.

4.1 Film Thickness: Spin Rate and Ink Concentration

The film thickness is measured by using the Dektak profilometer. A smooth film surface and a flat substrate are usually required to have a reliable thickness measurement. The films are deposited onto a Kapton substrate, which is flexible and can be easily curved. A bending of the substrate during spin coating can accumulate Si-NCs around the substrate edge which leads to poor thickness homogeneity. This problem has been somewhat circumvented by gluing the Kapton substrate to a cover glass. A batch of Si-NC films has been carefully prepared (from ultrasonic dispersed Si inks) in this way to study the dependence of the film thickness on the spin rate and the ink concentration.

To perform the thickness measurement, a scratch was made on the films to expose the substrate, and then the profilometer is applied to scan across the border between the area of the film surface and the substrate, so that the change of the surface profile is measured and the film thickness can be estimated. Typical example of the measurement data is shown in Fig. 4.1. It can be seen that the thickness is estimated from the vertical depth from the substrate to the film surface, which is about 750±150 nm. The film shows a rough surface and the error range is estimated from the amplitude of the variation of the height profile over the film surface.

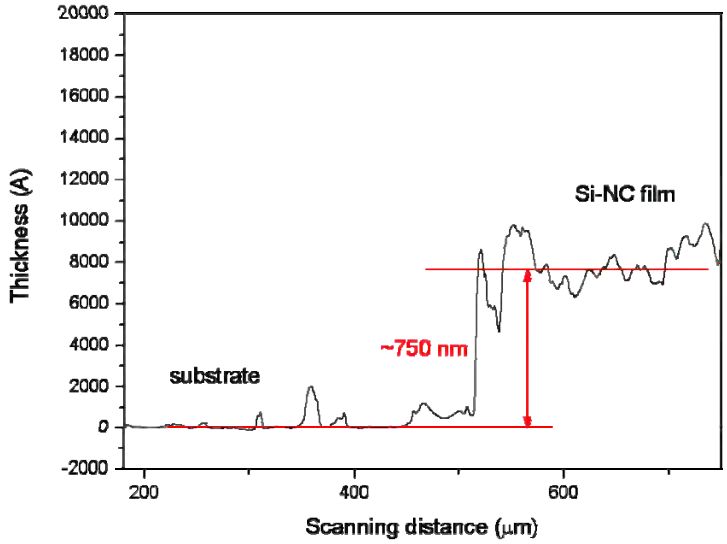

Fig. 4.1 Film thickness is estimated based on the surface profile change from the substrate to the film. The film is prepared with the ultrasonic dispersed Si ink (4.5 h, concentration 4.32 %, 40 μl). The spin rate is at 1000 rpm and spin time 40 sec.

The physics behind spin coating involve a balance between centrifugal forces and viscous forces which are determined by the viscosity of the mixture [1]. Two variable process parameters of study interest are: spin rate and ink concentration. The spin rate controls the centrifugal forces, while the ink concentration influences the liquid viscosity. The films prepared with different spinning rates (from 700 to 3500 rpm) and ink concentrations (from about 2 to 8 wt.%) are compared in terms of thickness. All the samples are prepared at room temperature with same amount of Si ink (40 μl) and with the spinning time of 40 seconds.

Figure 4.2 shows the changes of the measured film thickness as a function of the spinning rate and the ink concentration. As expected, the film thickness increases and decreases with the ink concentration and the spinning rate, respectively. Power law equations have been empirically used to fit these dependencies [1]:

$$D \sim v^m \qquad \text{(Eq. 4.1)}$$

$$D \sim (\text{Si-NC\%})^n \qquad \text{(Eq. 4.2)}$$

where D is the film thickness, v the spinning rate, and Si-NC% the ink concentration. In most applications, the film thickness varies with the square root of the spin rate (m = -0.5)

and *n* changes depending on the solution to be deposited [1]. In our case, it is found that the Eq. 4.1 and 4.2 fit well with the data in Fig 4.2a and b when m = -0.56 and n = 1.53, respectively.

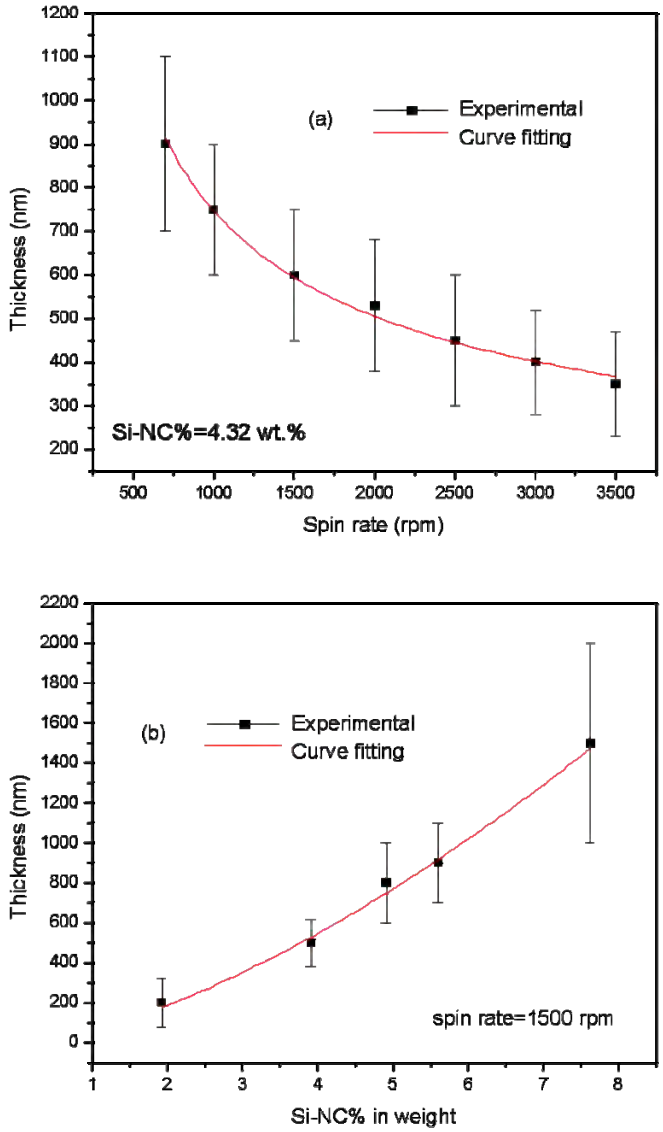

Fig. 4.2 Film thickness changes with (a) spin rate and (b) ink concentration. The error range is estimated from the amplitude of the variation of the height profile over the film surface.

For further film preparation, the spin rate 1500 rpm is used to have a moderate film thickness. An appropriate ink concentration needs to be determined also in consideration of the film morphology, which will be discussed in the next section 4.2.

4.2 Morphology: Ink Concentration and Dispersion Method

The morphology of the films was characterized by using SEM. A gold layer was deposited on the Kapton substrate before deposition of the Si-NC films to increase the electrical conductivity across the film and reduce surface charging during the measurement.

The Si-NC films produced from Si inks show a porous network made of spherical Si-NCs (as shown in Fig. 4.3). The average particle diameter is ~ 45nm.

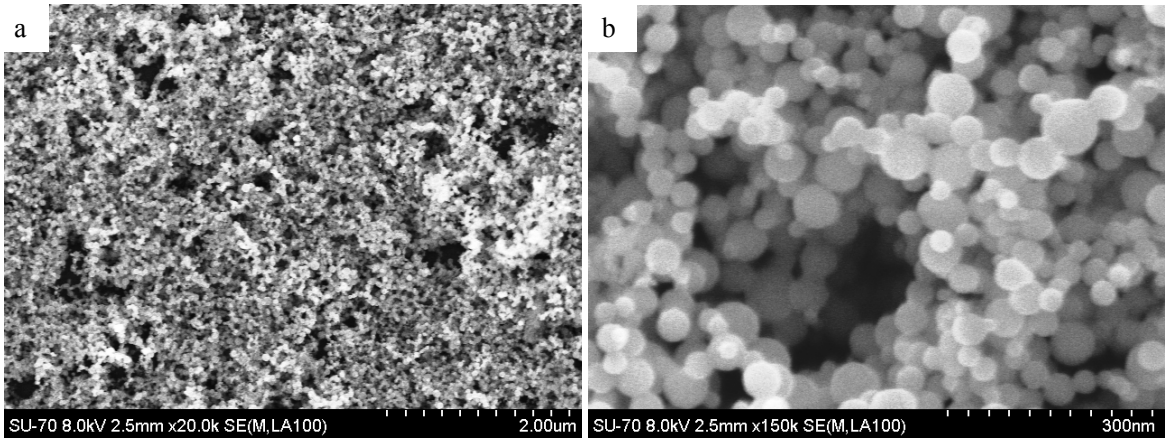

Fig. 4.3 Morphology of Si-NC films; (a) and (b) are SEM images with two different magnifications. The sample was prepared from ultrasonic dispersed Si inks (dispersed 4.5 h, 4.32 wt.% in concentration, 40 µl in volume); spin rate 1500 rpm, spin time 40 sec.

The ink concentration determines the viscosity of the ink, which influences the ultrasonic dispersion and the spin coating process and further the film morphology. Thus, to select a suitable ink concentration using the ultrasonication method, the films prepared from Si inks with different concentrations (1.92, 4.91 and 7.62 wt.%) are compared in morphology. As shown in Fig. 4.4, the diluted ink (1.92 wt.%) forms a sparse Si-NC network and poor coverage over the substrate (Fig. 4.4a and b), whereas the concentrated mixture (7.62 wt.%) results in many agglomerations of Si-NCs (Fig. 4.4e and f). The films produced from the ink with 4.91 wt.% Si-NCs show sufficient coverage and relative homogenous distribution (Fig. 4.4c and d). Therefore, this concentration (~5 wt.%) is used for further preparation of Si inks.

Additionally, Si-NC films prepared from Si inks with the concentration of ~5 wt.% are characterized using AFM to study their surface roughness. Figure 4.5 shows two and

three dimensional images of the film surface as scanned by using AFM and the corresponding statistic height distributions of all the points measured in the scanning area.

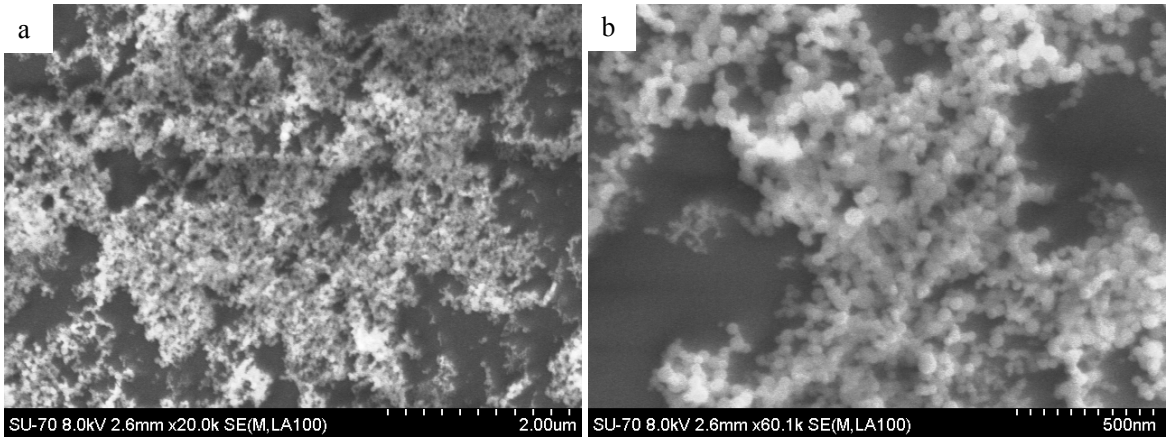

(a, b) Ink concentration = 1.92 wt.%

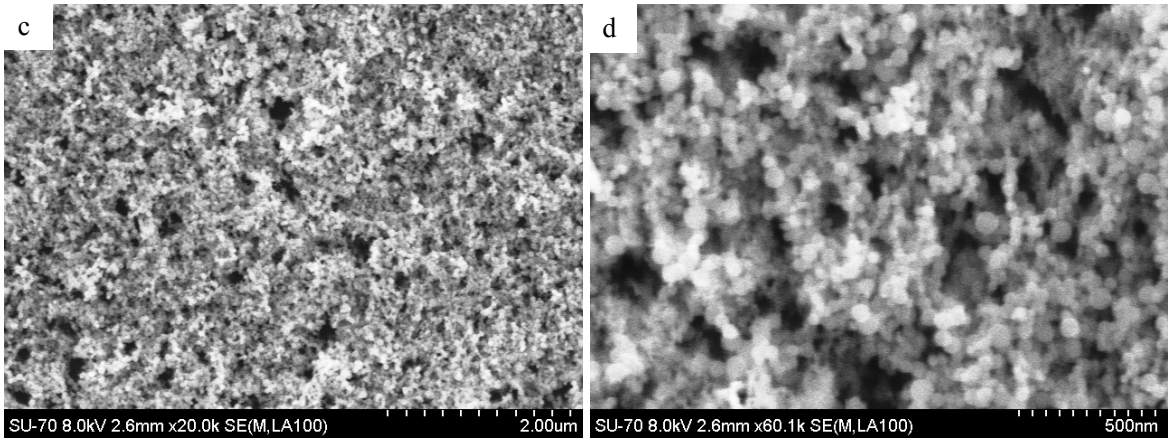

(c, d) Ink concentration = 4.91 wt.%

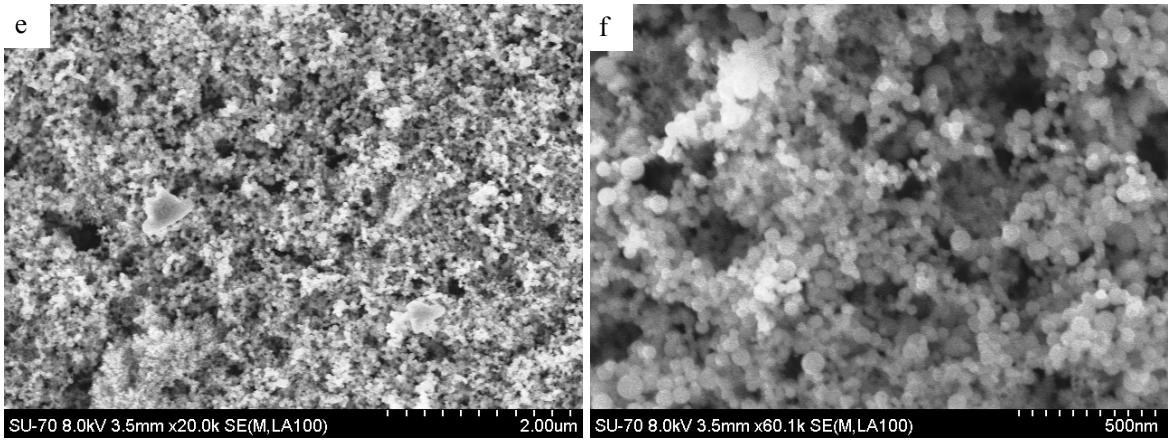

(e, f) Ink concentration = 7.62 wt.%

Fig. 4.4 Influence of the ink concentration on the surface morphology. All the films are prepared from ultrasonic dispersed Si inks (4.5 hours dispersed, 40 µl); spin rate 1500 rpm, spin time 40 sec.

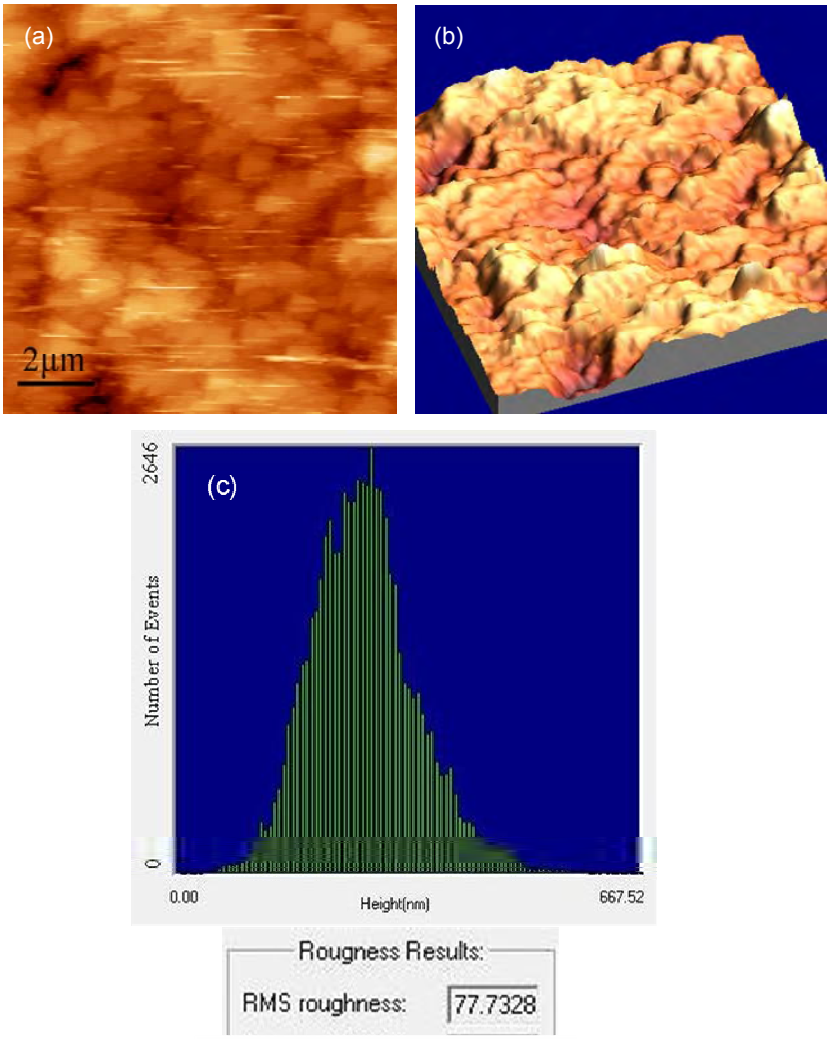

Fig. 4.5 AFM images of the Si-NCs films and corresponding surface roughness analysis
(a) two dimensional AFM image (b) corresponding three dimensional plot
(c) statistic distribution of the height of the surface points in the scanning area (scanning distance:10μm)
The RMS roughness (*Rrms*) is ~80 nm
The film was spin coated with ultrasonic dispersed Si ink (4.52 wt.% in concentration, dispersed 4.5 h, 40 μl in volume, spin rate 1500 rpm, spin time 40 sec.)

Here, the so-called root mean squared roughness (denoted as *Rrms*) is applied to determine the film roughness [2]:

$$Rrms = \sqrt{\frac{1}{n}\sum_{i=1}^{n}(y_i - \bar{y})^2}\ , \qquad \text{(Eq. 4.1)}$$

where, n is the number of points measured in a certain scanning distance, y_i is the vertical height of the ith point and $\bar{y}$ the average height of all the points. The *Rrms* indicates the

vertical deviations of the roughness profile from the mean vertical height. In case of Si-NC films prepared from ultrasonic dispersed ink (4.52 wt.% in concentration, spin rate 1500 rpm), the *Rrms* value is found to be ~ 80 nm (Fig. 4.5c), which is 10-15 % of the film thickness (~ 650 nm).

It can be seen from Fig. 4.5a that particles and voids in a size of hundreds of nanometers are present in the film, which correspond to "hills" and "valleys" respectively in the three dimensional plot (Fig. 4.5b). Our Si-NCs are in a diameter of ~ 45 nm. To further identify these structures, it is worth to compare the three dimensional AFM image (Fig. 4.5b) with a SEM image (Fig. 4.6): those "hills" and "valleys" of several hundreds nanometers in the three dimensional plot correspond to the assemblies of Si-NCs and voids at similar scale, respectively, in the SEM image (Fig. 4.6).

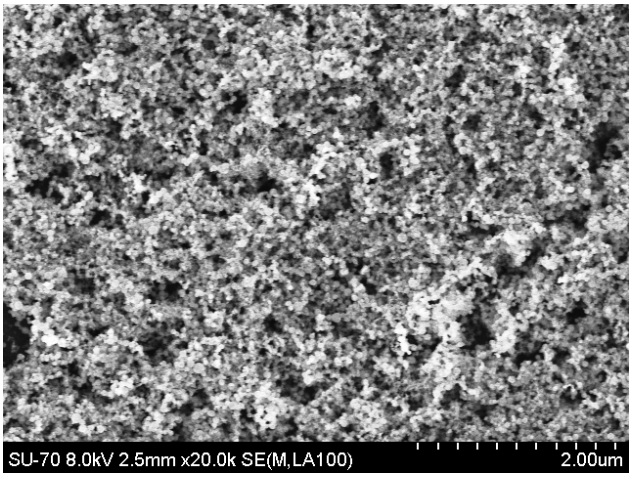

Fig. 4.6 A SEM image of the Si-NC film used for the roughness analysis.
The film was spin coated with ultrasonic dispersed Si inks (about 4.52 wt.% in concentration, 4.5 h dispersed, 40 µl in volume, spin rate 1500 rpm, spin time 40 sec.);

Figure 4.7 compares the morphology of films produced from the ultrasonic dispersed and ball milled Si inks. From Fig. 4.7a (a SEM image with a lower magnification, a broad field of view), we find that some agglomerates of Si-NCs (in a size of several µm) are present in the film, where the Si ink has been only ultrasonic dispersed for about 5 minutes. After 4.5 hours ultrasonic treatment, the Si-NCs are further dispersed, but still a few aggregations can be observed (Fig. 4.7c). The ball milled Si inks (4.5 hours) seem to be somewhat better dispersed than the ultrasonic dispersed inks and the resulting films have less and smaller agglomerates of Si-NCs (Fig. 4.7e). Additionally, it can be seen from Fig.

4.7d and f (images with a higher magnification) that both dispersion methods do not change the shape of Si-NCs.

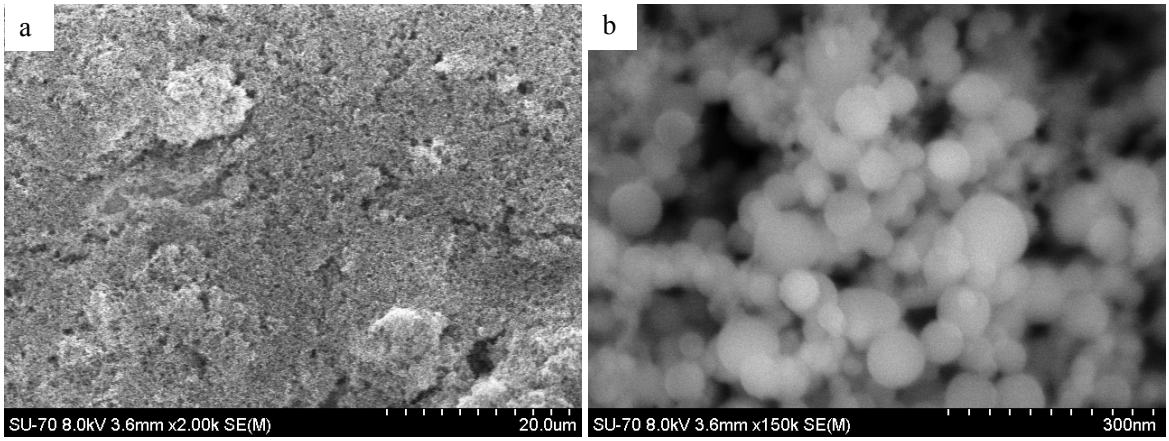

(a, b) ultrasonic dispersed for about 5 min.

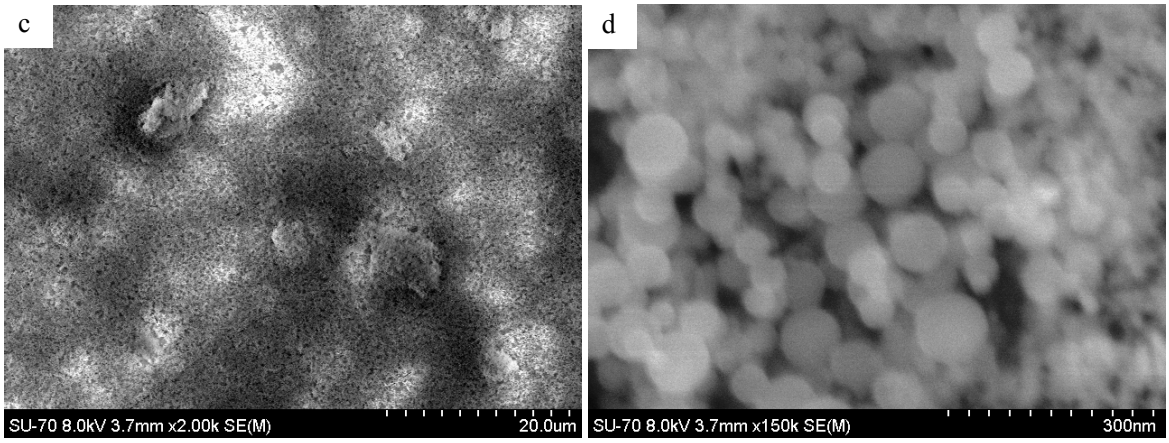

(c, d) ultrasonic dispersed for about 4.5 hours

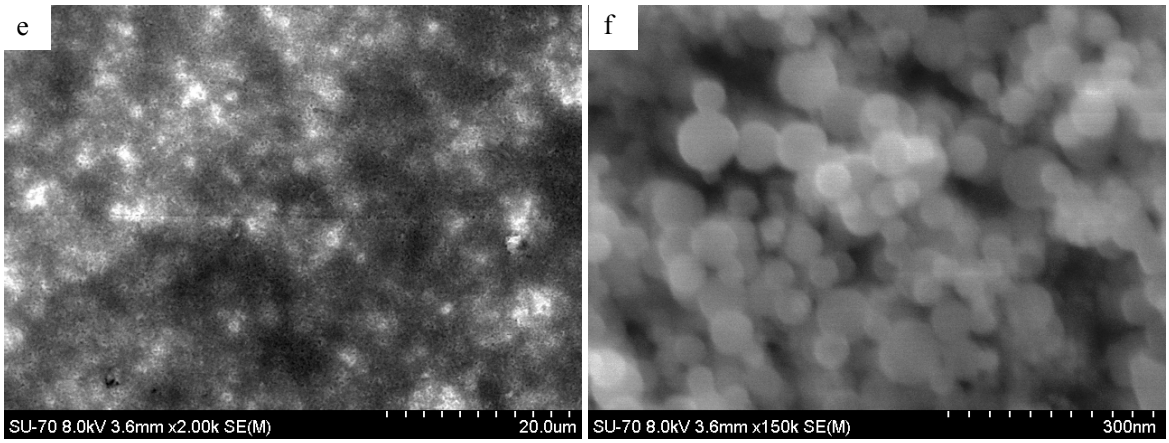

(e, f) ball milled for about 4.5 hours.

Fig. 4.7 Si-NC films produced from the ultrasonic dispersed and the ball milled Si inks.

Note that the bright spots in the images are caused by charging of the surface during the measurement.

The ink concentration is ~5 wt.%, 40 µl in volume; Spin rate 1500 rpm, spin time 40 sec.

4.3 Influence of HF Etching

Si-NC films were dipped into a diluted HF acid solution for 10 seconds to remove the surface oxides of Si-NCs. During this process, a partial amount of Si-NCs can be washed away, resulting in a decrease of the film thickness (30-50 % decrease was estimated by Dektak profilometer analysis). The morphology of the Si-NC films before and after the HF treatment is shown in Fig. 4.8. As can be seen, before HF etching (Fig. 4.8a and b), the film is formed by randomly distributed spherical Si-NCs, with voids presented in the network. After HF etching (Fig. 4.8c and d), the particle surface becomes more rough, and some particles seem to be connected with each other. The Si-NCs are somewhat more densely packed in comparison to that observed before HF etching.

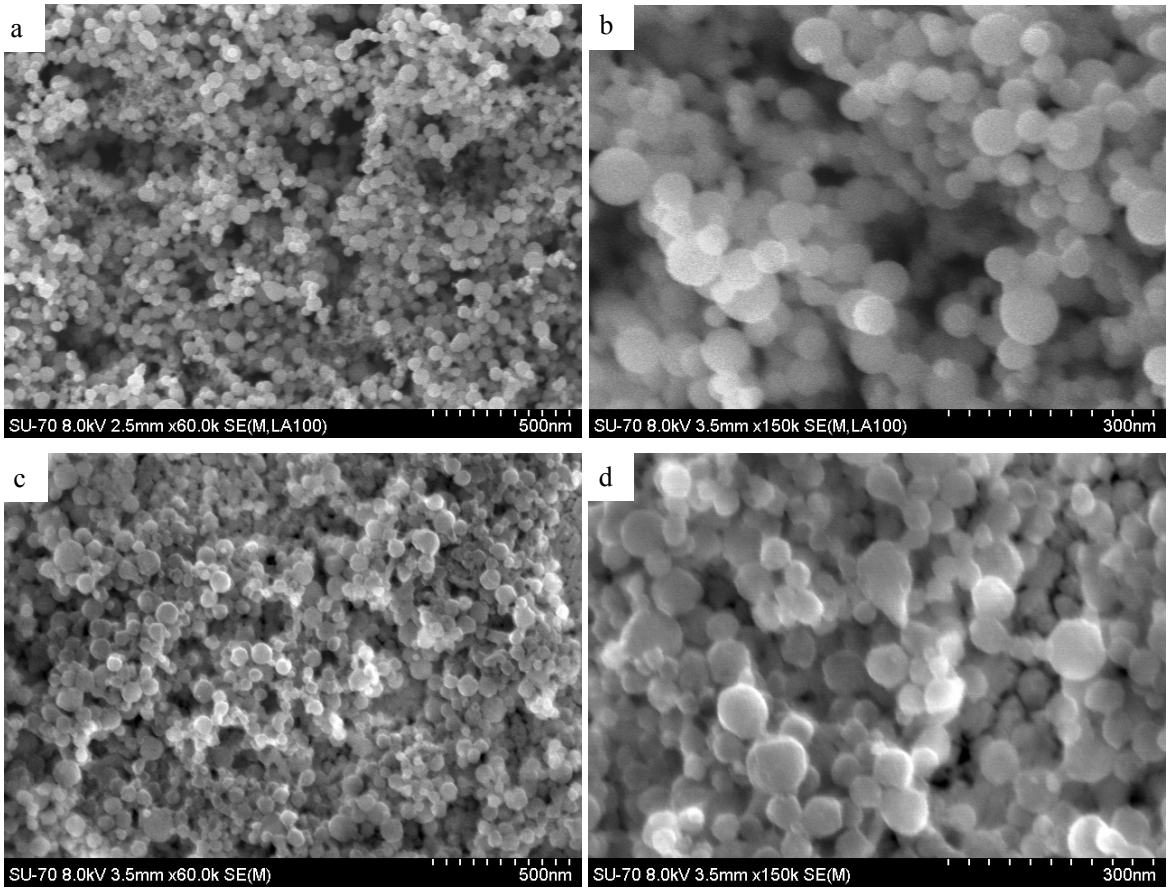

Fig. 4.8 Surface morphology of Si-NC films: (a, b) before HF etching; (c, d) after HF etching. Films prepared from ultrasonic dispersed Si ink with concentration ~5 %, 4.5h dispersion; spin rate 1500 rpm, spin time 40 sec.

4.4 References

[1] Retrieved from http://www.cpmt.org/mm/pkglab/theory/spin_theory.html (2009)

[2] Retrieved from http://en.wikipedia.org/wiki/Roughness (2009)

5 Electrical Measurements

In this chapter, the results of the electrical measurements will be presented and discussed as follows. Firstly, we start with the electrical properties of the intrinsic Si-NC films, including their conductivity-time (σ-t) and current-voltage (I-V) characteristics before and after the HF etching procedure. Here films before HF etching are called as-deposited films. Afterwards, the properties of the P-doped films are discussed, with an emphasis on the ambient degradation of the conductivity after HF etching. Then the influence of the methods of dispersing Si inks on the σ-t behaviour is discussed. Comparisons will be made between samples produced from the ultrasonic dispersed and the ball milled Si inks. The photoconductivity of the Si-NC films is discussed in the last section.

5.1 Conductivity of the Intrinsic Si-NC Films

5.1.1 As-deposited Films

The σ-t curves of the as deposited intrinsic Si-NC films (average diameter of Si-NCs 46.8 nm) were measured at ambient air atmosphere and room temperature by a continuous application of a DC voltage at 80V (for 28 min.). As shown in Fig. 5.1a, the conductivity decreases from a value of 6×10^{-9} $\Omega^{-1}cm^{-1}$, followed by a saturation at a lower value of $\sim2\times10^{-9}$ $\Omega^{-1}cm^{-1}$.

After removal of the applied voltage and waiting for about one hour, another σ-t measurement was performed. It is found that the conductivity is recovered to the level of the starting value, and again decreases until it reaches the saturation (Fig. 5.1b). This indicates that the initial fast decay is not permanent. In a discrete measurement, where the DC voltage applied in an interval of about 4 min, only a slight decrease of the conductivity can be observed from 6.8×10^{-9} to 6×10^{-9} $\Omega^{-1}cm^{-1}$ (Fig. 5.1c) in a period (of ~30 min.) similar to the continuous DC voltage measurement, which suggests that the fast decay in Fig. 5.1a and b is due to the application of the DC voltage.

One possible explanation is that the conductivity changes are caused by the thermal heating of the sample during the measurement. In a semiconductor, an increase of the temperature normally leads to an increase of the conductivity, due to thermal excitation of

charge carriers to the conduction and/or valence band. Since we see a decrease of the conductivity, this is not the effect that may describe our observation. It has been reported that surface adsorption (or desorption) effects caused by the local heating can alter the surface potential of semiconductors thereby changing the electrical properties [1, 2]. According to Tanielian, an accumulation layer of air molecules (such as water) adjacent to the surface of intrinsic and n-type amorphous Si films can lead to conductivity changes [3]. In his study, similar conductivity decay was also recorded during the σ-t measurements of amorphous Si at ambient conditions. Considering the fact that such a decay was not observed in the previous studies at vacuum condition [4], probably, during the measurement of our samples, a desorption of air molecules due to local heating leads to the decrease of the conductivity when the voltage is applied continuously.

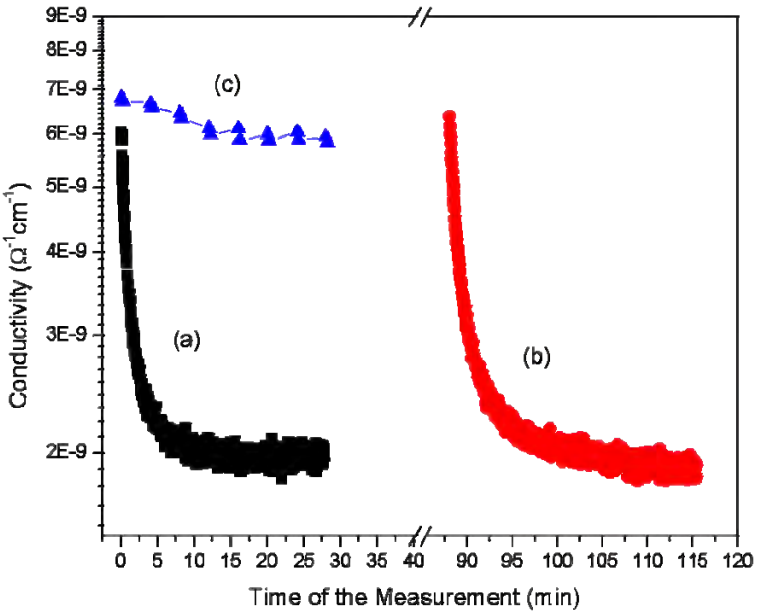

Fig. 5.1 σ-t curves of the intrinsic Si-NC film in a log Y-X plot

(a). Continuous application of the voltage for about 28 min. (b) Measurement was performed after 1 hour break (removal of the voltage). (c) Voltage applied discretely with an interval of about 4 min.

Fig. 5.2a shows a group of short I-t measurements (20 sec. each) of an intrinsic Si-NC film with increasing applied voltage. The corresponding I-V curves (Fig. 5.2b) are then plotted based on the average current of the short I-t measurement at each voltage. In these measurements the time window of application of voltage is short enough that the decrease over time due to the continuous application of voltage is negligible. It can be seen from Fig. 5.2b that the current increases with the voltage from 20 to 80 V, which can be described by

a power law dependence $I \sim V^m$, with m = 1.68. This value is quite close to that reported by Rafiq et al. [5], where m = 1.8 at 300 K in undoped Si-NC films (refer to section 2.2.1). Their Si-NCs were also grown from gas phase with an average particle size of ~8 nm and a surface SiO_2 layer of 1-2 nm. According to these authors [5], the power law I-V dependence observed from Si-NC films is consistent with the SCLC model of conduction. We will discuss this further in the next section 5.1.2.

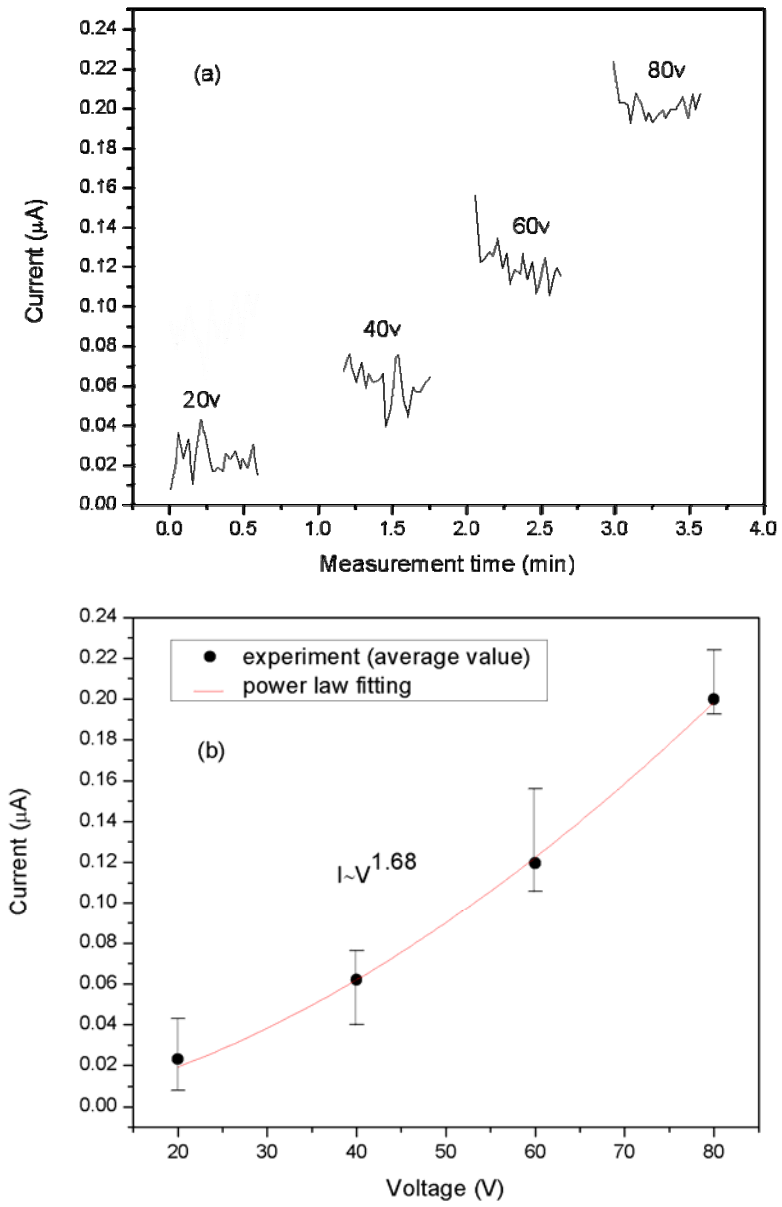

Fig. 5.2 I-V characteristic of the as-deposited intrinsic Si-NC film.

(a) a group of short I-t measurements and (b) corresponding I-V curve and power law fitting. The dots indicate the average current, whereas the upper and lower error bars indicate the maximum and the minimum current, respectively, measured at each applied voltage.

5.1.2 After HF Etching

In order to improve the electrical conductivity of the intrinsic Si-NC films, the films were etched in a diluted HF solution (5%) to remove the native oxide layer of the Si-NCs (refer to section 3.1.4). After this treatment, the films were kept all the time at ambient conditions. Figure 5.3 compares the conductivity of an intrinsic Si-NC film before and after HF treatment. It can be seen that before HF etching all the σ-t curves show similar features as discussed above, i.e., a fast decrease in the beginning and saturation at a lower level (~2×10^{-9} $\Omega^{-1}cm^{-1}$).

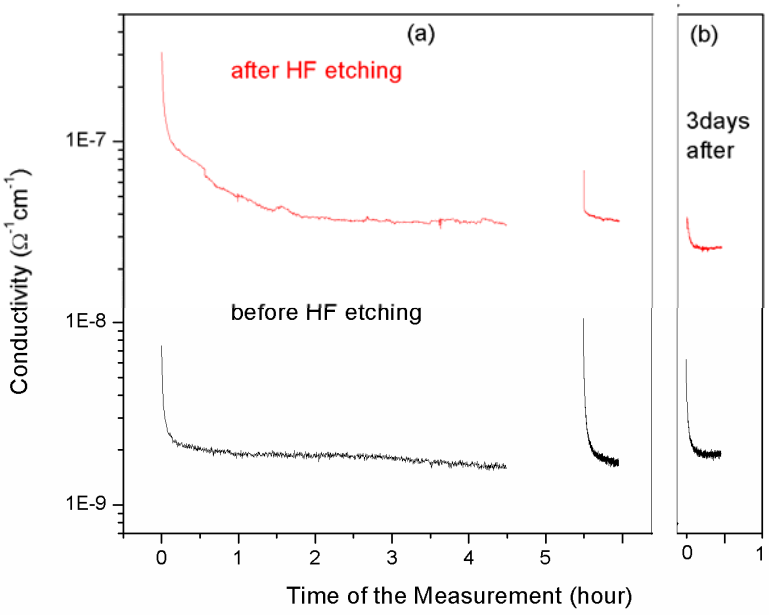

Fig. 5.3 Conductivity of the intrinsic sample measured before and after HF etching.
The measurements of the HF-etched sample have started about 5 min (sample handling) after the HF etching procedure.

After HF treatment, the initial value of the conductivity (3×10^{-7} $\Omega^{-1}cm^{-1}$) is much higher than that observed before HF etching (7×10^{-9} $\Omega^{-1}cm^{-1}$), as shown in Fig. 5.3a. Such an improvement can be attributed to the removal of the native oxide which impedes the transport of electrical carriers. Besides, a morphology effect can also contribute to the conductivity increase. We have seen in Fig. 4.8 that the Si-NCs become more densely packed and connected after the HF treatment. This may provide a more efficient topological network for carrier transport, resulting in a higher macroscopic electrical conductivity.

The conductivity of the HF-etched film degrades rapidly from the initial value (3×10^{-7} $\Omega^{-1}cm^{-1}$) to about 4×10^{-8} $\Omega^{-1}cm^{-1}$ in the first two hours of air exposure and continuous application of voltage (Fig. 5.3a). After one hour break of the measurement, while the recovery of the conductivity in the intrinsic sample is complete, the recovery in the case of the HF-etched film is only partial. This indicates that the degradation of the conductivity in the case of the HF-etched films is in part permanent, most probably due to oxidation of Si-NCs. We believe both the reversible effect of the applied voltage as discussed before and the oxidation of Si-NCs contribute to the observed conductivity decay. The former effect reduces the conductivity rapidly in the first several minutes after the measurement starts, whereas the latter one takes place all the time at ambient conditions and the corresponding conductivity decrease is irreversible.

After three days storage at ambient conditions, we have measured the σ-t curve again, and the results are shown in Fig. 5.3b. As can be seen, the sample before HF etching shows similar conductivity levels, whereas the conductivity at saturation of the HF etched film is lower than the value measured three days before, which could be attributed to the oxidation of Si-NCs.

In addition, it is worth to compare our measurement with those reported by Stegner et al. [4]. We found that the conductivity of the HF-etched intrinsic samples in our work (from 3×10^{-7} to 4×10^{-8} $\Omega^{-1}cm^{-1}$) are much higher than their measurement in reference [4], where the conductivity of the intrinsic Si-NC film (mean diameter of Si-NCs of 30 nm) is $\sim10^{-10}$ $\Omega^{-1}cm^{-1}$ as measured in vacuum after HF etching. Our Si-NCs with larger size (~45 nm) might provide paths to electrical carriers with less resistance [6], and the ambient environment might also change the surface potential of semiconductor crystals due to the presence of various surface adsorbates in air [3], resulting in the higher conductivities as observed in our experiments.

To monitor the conductivity changes over longer time of exposure to air, further σ-t measurements (about 28 min. each) were performed for about 25 days after HF etching. The data from these measurements are shown in Fig. 5.4a, resulting in a plot of the conductivity changes as a function of the exposure time to air shown in Fig. 5.4b. We have seen above that the application of voltage leads to a conductivity decrease. To exclude this

effect, the data points in Fig. 5.4b correspond to the conductivity at the lower range of each σ-t curve (where the conductivity saturates at a lower value) in Fig. 5.4a.

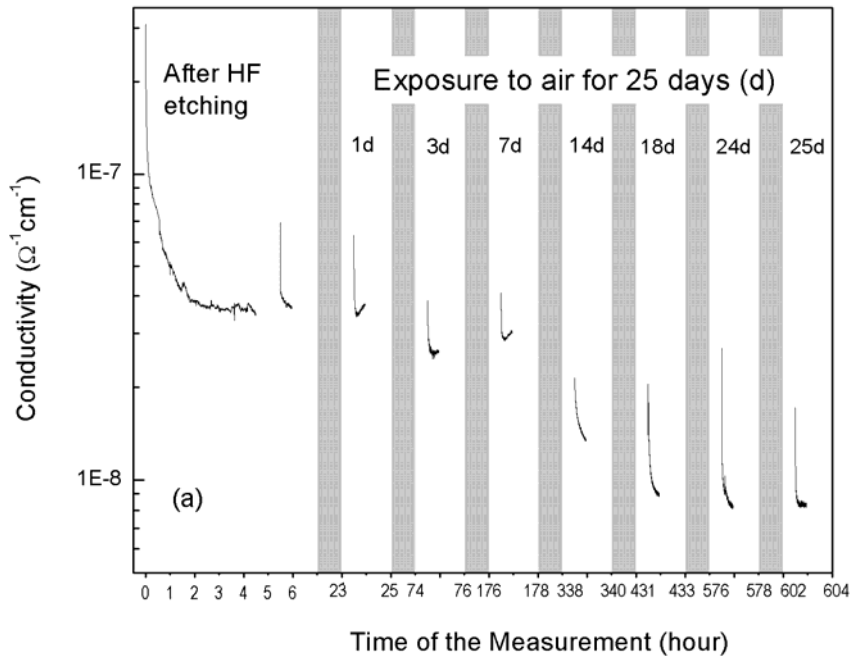

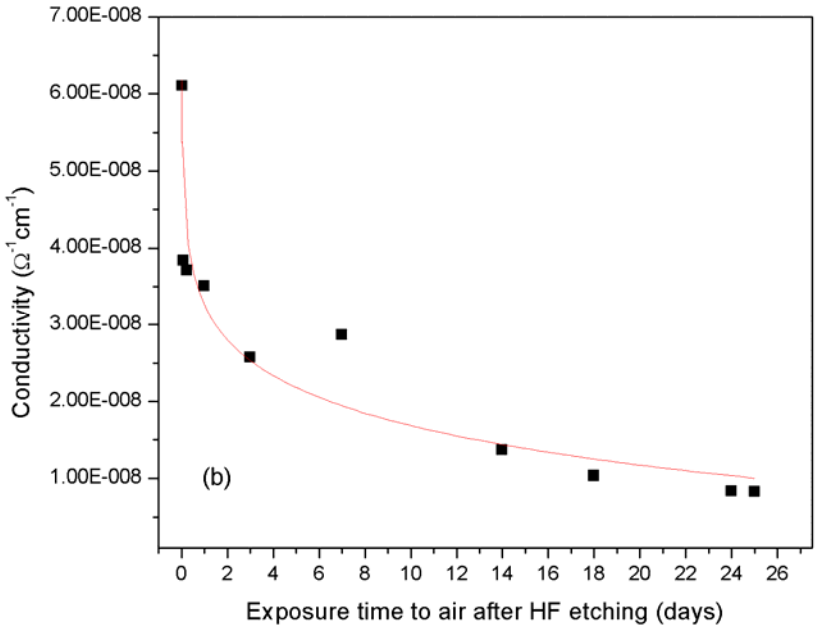

Fig. 5.4 Conductivity changes of the intrinsic Si-NC film after HF etching and exposure in air for 25 days. (a) σ-t curves measurements after HF etching, plotted in a log Y-X scale; (b) the corresponding linear plot of the conductivity changes as a function of the exposure time after HF etching. The solid line (in red) is a guide to the eyes.

It can be seen from Fig. 5.4b that a rapid decrease of the conductivity occurs within the first 3 days after the HF treatment. The conductivity keeps on degrading afterwards, but the rate of the change seems to be smaller. This might be correlated with the surface oxidation of nanometer-sized Si, which is reported to be a self-limited process [7], [8]. We will come back to this point in Chapter 6, where the oxidation kinetics will be studied by means of FT-IR spectroscopy. Additionally, it is interesting to notice that the conductivity 25 days after air exposure (8.3×10^{-9} $\Omega^{-1}cm^{-1}$) is still much higher than that measured before HF treatment (which saturates at ~2×10^{-9} $\Omega^{-1}cm^{-1}$, Fig. 5.3).

Figure 5.5b shows the I-V curve of an intrinsic Si-NC film measured 7 hours after HF etching. Again, this curve is plotted based on a group of short I-t measurements (Fig. 5.5a), as described above. It can be seen that the I-V curve has a strong non-linear shape, which can also be described by the power law dependence, $I \sim V^m$. However, the power exponent (m = 3.15) is larger than that obtained before HF treatment (m = 1.68).

The power law $I \sim V^m$ dependence might be interpreted by the SCLC theory. SCLC can occur in highly insulating materials when carriers are injected and non-compensated charge is present. The current is determined by the number of free charge carriers in the interior space of the materials and the transient time (the average time for the free carriers move between the electrodes). They are generally described by [9]

$$I = aV + bV^m \qquad \text{(Eq. 5.1)}$$

The first term in Eq. 5.1 dominates at low fields, resulting in Ohmic behaviour, while at high fields the second term controls the I-V characteristics and the equation simplifies to $I \sim V^m$ (m>1). The parameter m can be related to the energetic distribution of localized states (carrier traps) in the materials: large values of m are indicative of a slowly varying energetic distribution of traps, resulting in a more uniform distribution of the space-charge density between cathode and anode [10].

The value m obtained in our study is comparable with other reported values ranging from 1.8 to 4 regarding various Si nanocrystal systems [5], [6] and [11]. The large value m in the HF-etched film might be understood qualitatively by the removal of the energetic barriers of surface oxide between Si-NCs after the HF treatment, which allows the charge

carriers to move through a more uniform energetic distribution of the traps (corresponds to large *m*), assuming the Si-NCs are carrier trapping sites in the films [5].

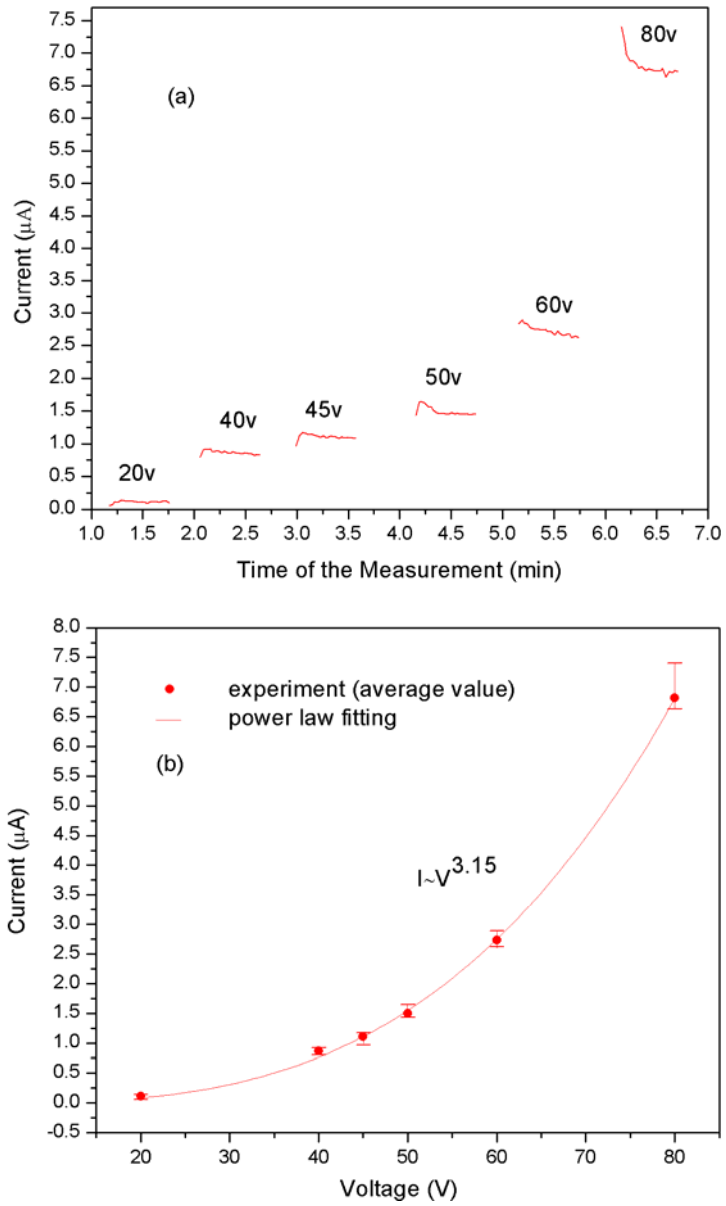

Fig. 5.5 I-V curve of the intrinsic Si-NC film measured 7 hours after HF etching.
(a) a group of short I-t measurements and (b) corresponding I-V curve and power law fitting
The dots indicate the average current, whereas the upper and lower error bars indicate the maximum and the minimum current measured at each applied voltage.

Apart from SCLC theory, non-thermal tunnelling mechanisms (typically Fowler-Nordheim tunnelling theory) can also be used to describe the non-linear I-V curve of the

HF-etched films (with larger value *m*) [6]. As stated in section 2.2.1, the conduction mechanisms based on I-V analysis are controversial, which is beyond the scope of this thesis. Temperature–dependent I-V measurements can be carried out in the future, which may provide us further understanding concerning the I-V behaviour of our Si-NC films as well as the conduction mechanism.

5.2 Influence of Phosphorous Doping

Doping is considered to be effective in enhancing the conductivity of Si-NCs [12]. In this work, the electrical properties of films prepared with P-doped Si-NCs (5×10^{20} /cm^3) were studied by σ-t measurements both before and after the HF treatment. As shown in Fig. 5.6a, the P-doped samples also present a fast decay in the beginning of the σ-t measurement. Before the HF treatment, the conductivity of the P-doped film (2.5×10^{-9} Ω^{-1}cm^{-1}, at the saturation region) is quite close to that of the intrinsic sample (~2×10^{-9} Ω^{-1}cm^{-1}).

After HF etching (Fig. 5.6b), the conductivity of the P-doped sample increases significantly (from 2.5×10^{-9} to ~5×10^{-6} Ω^{-1}cm^{-1}). The value of 5×10^{-6} Ω^{-1}cm^{-1} is more than one order of magnitude higher than that measured for the intrinsic Si-NC film after HF etching (~3×10^{-7} Ω^{-1}cm^{-1}). This value is also higher in comparison to the conductivity of a P-doped film of Si-NCs reported in reference [4], where the conductivity is about 3×10^{-8} Ω^{-1}cm^{-1} (measured in vacuum after HF etching, average NC size 30 nm). We notice that their doping concentration of the Si-NCs (1.5×10^{20} /cm^3) is less than 1/3 of that used in our studies (5×10^{20} /cm^3), which might explain the higher conductivity obtained in our experiments. Besides, as stated before, the difference can also be attributed to the different nanocrystal sizes and the measurement conditions.

The evolution of σ-t curves of the P-doped film have been recorded for 25 days after HF etching and compared with the data obtained for intrinsic samples (Fig. 5.6b). The corresponding conductivity changes are then plotted as a function of the exposure time in Fig. 5.7. Generally, downward trends of the conductivity can be seen for both the P-doped and the intrinsic films, i.e., a fast decrease in the first 3 days followed by a slower degradation.

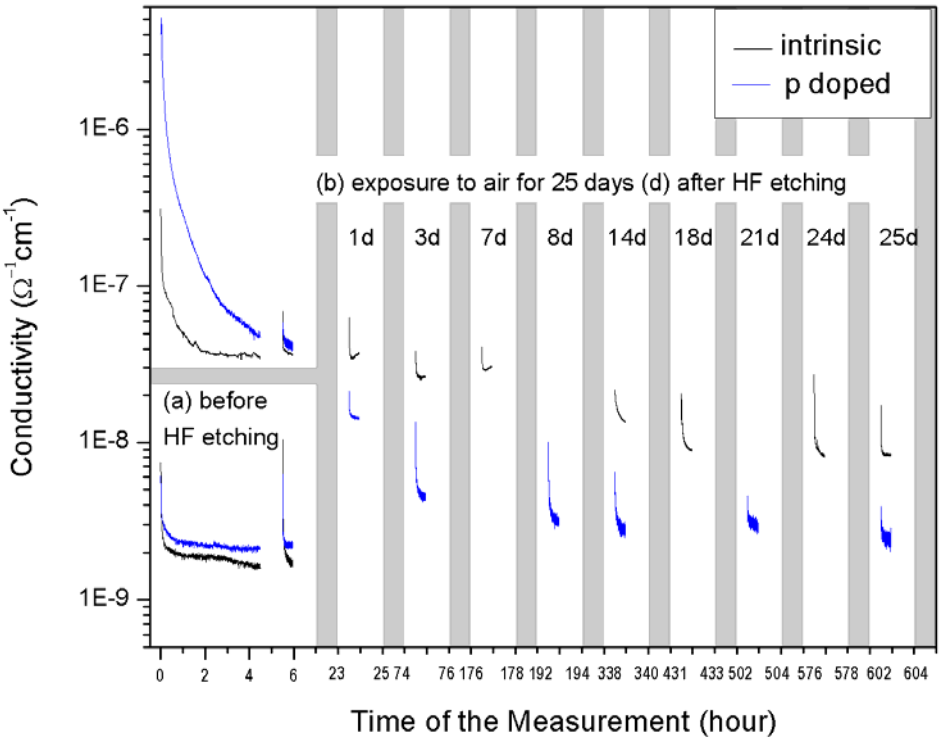

Fig. 5.6 Comparisons between the conductivities of the intrinsic and the P-doped Si-NC films (a) before HF etching; (b) 25 days exposure to air after HF etching.

The σ-t measurements are applied to monitor the conductivity degradation.

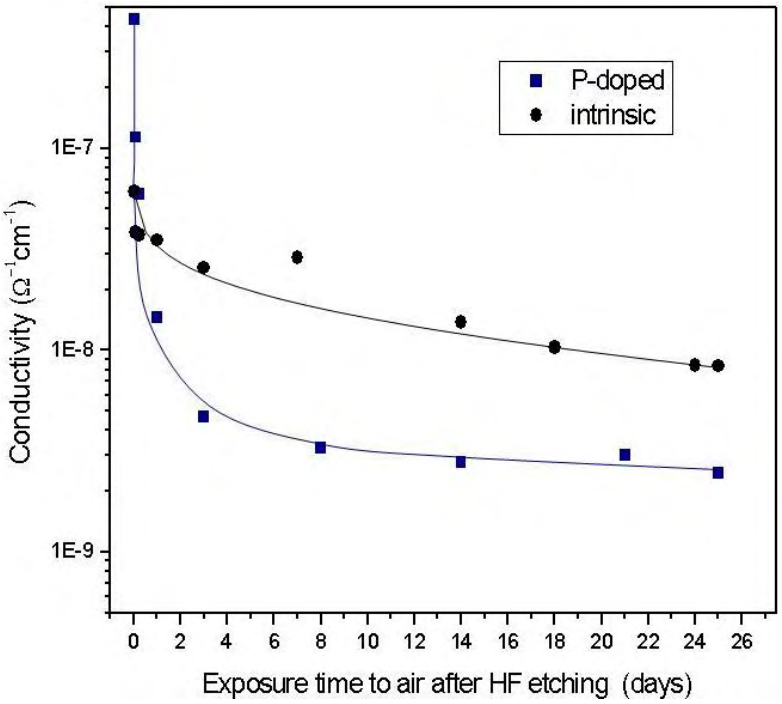

Fig. 5.7 Conductivity changes in a time scale of 25 days exposure to air after HF etching.

The date points correspond to the conductivities (lower range of the σ-t curves) in Fig. 5.6b.

The solid lines are guides to the eyes.

Furthermore, we found that the conductivity of the P doped sample decreases much more than that of the intrinsic film in the initial 3 days. After 25 days air exposure, the conductivity of the P-doped film already decreases to the level measured before HF etching, whereas the conductivity of the intrinsic sample is still higher than that recorded before the HF treatment (Fig. 5.6b). The observation of an enhanced rate of conductivity decrease as a function of oxidation time for the P-doped film may indicate that surface oxidation of P-doped Si-NCs is enhanced. This is consistent with recent first-principles calculations [13].

5.3 Influence of the Dispersion Method

Up to now, we have discussed the electrical properties of both the intrinsic and the P-doped Si-NC films, prepared from the ultrasonic dispersed Si inks. The ball milling process has been found to be effective to disperse the Si-NCs [12], [14]. In this section, we will compare the electrical properties of the Si-NC films prepared from the Si inks dispersed by these two methods. The σ-t characteristics are measured both before and after the HF treatment. The results are shown in Fig. 5.8a and b, respectively. It can be seen that the voltage-induced decrease in conductivity is observed in all the measurements of the films. For all the as-deposited films (before HF etching), the conductivity saturates at similar levels in the range 1- 3×10^{-9} $\Omega^{-1}cm^{-1}$. It seems that the films prepared from the ultrasonic dispersed Si-NCs are slightly more conductive than those from the ball milled Si-NCs (both the P-doped and the intrinsic). After the HF treatment (Fig. 5.8b), the films prepared through the two different dispersion methods, present similar conductivity levels and σ-t curves.

Pereira et al. found [14] that the ball milling process generates Si-dbs on the surface of Si-NCs, which can compensate the charge carriers and deteriorate the conductivity of Si-NC films. However, we found that the Si-NC films prepared through the ball milling process show σ-t behaviour similar to the films prepared from ultrasonic dispersed Si inks, both before and after the HF treatment. One of the assumptions in this study is that the ultrasonication method has less impact on the Si-NCs; fewer surface defects generated during dispersion and thus less compensation of charge carriers in comparison to the ball milling process. It has also been shown in Fig. 4.7 that films produced from the ball milled

Si inks have a more homogenous distribution than from the ultrasonic dispersed Si inks, which might provide a better topological network for transport of charge carriers. The electronic and morphological effects may compensate each other, resulting in similar macroscopic electrical behaviour in the ball milled and ultrasonic dispersed Si-NC films.

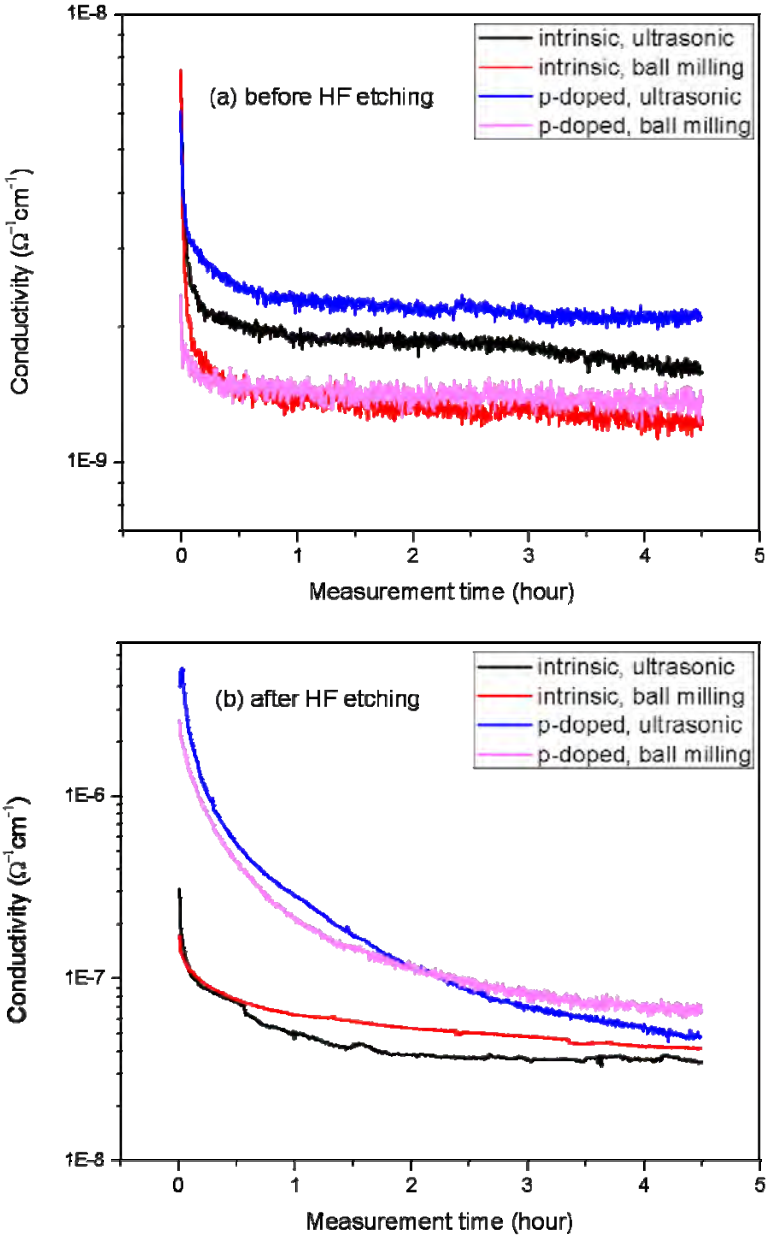

Fig. 5.8 σ-t curves of the intrinsic and p-doped samples with Si-NCs dispersed by ultrasonic and ball milling processes. (a) measured before HF etching; (b) measured after HF etching.

5.4 Photo-induced Conductivity

The photoconductivity of the intrinsic Si-NC films (ultrasonic dispersed, before and after HF etching) has been investigated by using a halogen lamp with a power density of 100 W/cm^2 as illumination source. The resulting σ-t curves are compared with those measured in the dark in Fig. 5.9. Before HF etching, no significant difference between the dark and the photoconductivity is observed. In the case of the HF-etched film, the situation is completely different. Firstly, we measured the photoconductivity and the resulting σ-t curve saturates at ~8×10^{-8} Ω^{-1}cm^{-1}. Then, the measurement was switched between the dark and the photoconductivity. The corresponding σ-t curve shows a "step" feature, i.e., a lower value (~ 4×10^{-8} Ω^{-1}cm^{-1}) in the dark and a higher value (~8×10^{-8} Ω^{-1}cm^{-1}) during illumination. Finally, a dark σ-t curve was recorded, which also saturates at ~ 4×10^{-8} Ω^{-1}cm^{-1}. The photoconductivity is about two times higher than the conductivity measured in the dark.

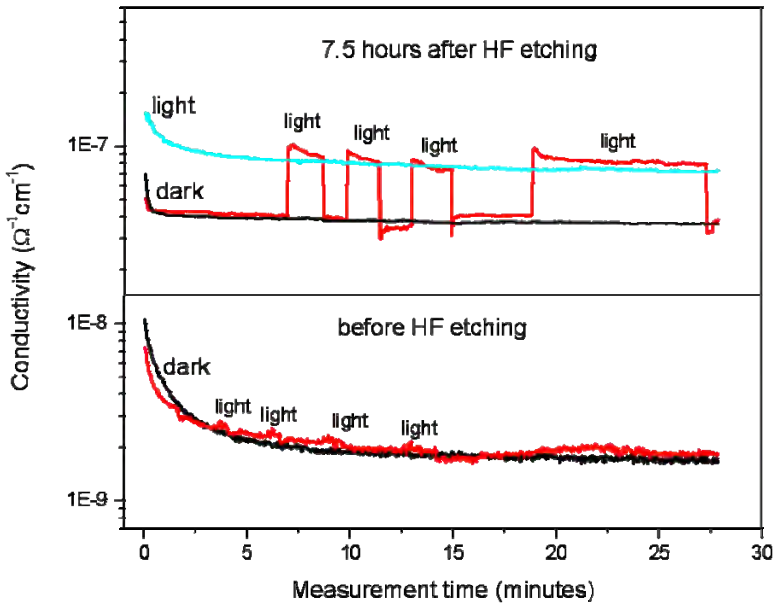

Fig. 5.9 Influence of the light exposure on the conductivity of intrinsic Si-NC films before and after HF etching.

It is interesting to compare the photoconductivity of the HF-etched films obtained from our experiments with the values reported by Pradhan et al. [15]. In their work, the photoconductivity of LB monolayers of Si-NCs (core diameter 3.86 ± 0.85 nm, coated with a siloxane-structure) were measured in vacuum by exposure to four different lasers (red,

green, blue and UV, refer to section 2.2.3). They found that an enhanced conductivity by illumination can be seen when exposed to photoexcitation with photon energy greater than the effective particle bandgap (green laser wavelength, 532nm). Typically, at room temperature, the photoconductivity is 1.3×10^{-6} $\Omega^{-1}cm^{-1}$ (illuminated by blue laser) and 1.9×10^{-6} $\Omega^{-1}cm^{-1}$ (illuminated by UV laser), which is about 1.7 and 2.5 times higher than the dark conductivity (7.5×10^{-7} $\Omega^{-1}cm^{-1}$), respectively. We note that at room temperature the photoconductivity is about two times higher than the dark conductivity in both our experiments and reported by Pradhan et al. However, the absolute values of conductivity measured for the LB monolayers are about one order of magnitude higher than for our Si-NC films. We believe that this difference could be due to higher conductivity for electron transport that is obtained in the LB monolayers, which show a hexagonal-type structure with Si-NCs densely packed and each Si-NC is in contact with six other Si-NCs (refer to Fig. 2.4). Besides, other effects such as the surface condition of Si-NCs might also account for the conductivity difference between these two works.

5.5 Conduction Mechanisms of Si-NC films

Based on the above experimental results, we can have the following discussion regarding the electrical conduction mechanisms in the Si-NC films. Before HF etching, neither the light exposure nor the P-doping leads to significant changes on the σ-t behaviour of Si-NC films (as shown in Fig. 5.9 and Fig. 5.6a, respectively). This means that the free charge carriers excited by illumination or ionized from the P dopant do not have a significant contribution to the electrical conduction in the Si-NC films. This could result from a strong suppression on the carrier mobility between Si-NCs caused by the potential barriers of surface oxide in each Si-NC. In other words, most of the photo generated or dopant ionized charge carriers are not “free” to move through the Si-NCs network and their contribution to the conductivity of Si-NC films is limited. Another mechanism, most probably the conduction induced by localized states on the surface of Si-NCs (or in the surface oxide layer) such as surface defects, plays a major role in the macroscopic conductivity of Si-NC films before HF etching. In fact, a recent study has demonstrated that hopping conduction between defect states (Si-dbs) occurs in Si-NC film in the dark [4], [14]. Various ambient adsorbates are also known to alter the surface potential of semiconductors resulting in changes in conductance [2], [3]. Moreover, the assumption of the surface conduction can

also explain other observations in this study. For example, a decrease of the conductivity caused by a continuous application of voltage (typically shown in Fig. 5.1), which can be explained by the change of surface adsorbates due to local heating during the measurement. Additionally, the conductivity obtained at ambient conditions in this study is higher than other reported measurements of Si-NC films in vacuum [4], [12], which partly indicates that the surface of the Si-NCs plays a major role in electrical conduction.

After HF etching, the potential barriers imposed by the surface oxide are removed, improving the mobility (e.g. tunnelling) of the charge carriers between "bulk" states inside the core of Si-NCs and enhancing the transport efficiency through the Si-NCs network. In this situation, the photo-generated or the dopant-ionized charge carriers can move through the Si-NC network more efficiently. The resulting increase of the conductivity is much larger than the contribution from the surface effect. Therefore, an enhanced conductivity by illumination or P-doping can be clearly observed after the HF treatment.

5.6 References

[1] S. Miyazaki, H. Nishimura, M. Fukuda, et al., Appl. Surf. Sci. 113/114 (1997) 585.

[2] W.H. Brattain, J. Bardeen, and Bell Syst. Tech. J. 32 (1953) 1.

[3] M.Tanielan, Philosophical Mag. Part B 45 (1982) 435.

[4] A.R. Stegner, R.N. Pereira, K. Klein, et al., Phys. Rev. Lett. 100 (2008) 026803.

[5] M.A. Rafiq, Y. Tsuchiya, H. Mizuta, et al., Appl. Phys. Lett. 87 (2005) 182101.

[6] T.A. Burr, A.A. Seraphin, E. Werwa, et al., Phy. Rev. B 56 (1997) 8.

[7] G. Ledoux, J. Gong, F. Huisken, et al., Phys. Rev. B 62 (2000) 15942.

[8] G. Ledoux, O. Guillois, D. Porterat, et al., Appl. Phys. Lett. 79 (2001) 4028.

[9] M.A. Lampert, P. Mark, Current Injection in Solids, Academic, New York, (1970).

[10] A. Rose, Phys. Rev. 97 (1955) 1538.

[11] H.W. Lau, and O.K. Tan, Appl. Phys. Lett. 89 (2006) 113119.

[12] R. Lechner, A.R. Stegner, R.N. Pereira, et al., J. Appl. Phys.104 (2008) 053701.

[13] L.C. Ciacchi and M.C. Payne, Phy. Rev. Lett. 95 (2005) 196101.

[14] R.N. Pereira, A.R. Stegnera, K. Klein, et al., Physica B 401-402 (2007) 527.

[15] S. Pradhan, S.W. Chen, J. Zou, et al., J. Phys. Chem. C 112 (2008) 13292.

6 FT-IR Studies

We have seen from the previous chapter that the HF etching process increases the electrical conductivity of the Si-NC films significantly and the conductivity degrades upon subsequent exposure of the films to ambient conditions. These results are considered to be related with the changes on the surface condition of the Si-NCs. It has been demonstrated that FT-IR spectroscopy can be used to characterize the surface state of Si-NCs and the IR spectra of the as grown, HF etched, and re-oxidized (in 12 days) Si-NCs films have been observed and discussed [1], [2]. However, the oxidation kinetics of the Si-NCs after HF etching has not yet been fully understood. In this chapter, an investigation of the oxidation kinetics is presented based on the evolution of IR spectra of HF etched Si-NCs, which provide us a further understanding of the electrical behaviour of the Si-NC films.

Firstly, we will compare the IR spectra from the Si-NC films measured before and after HF etching as well as that measured after exposure to ambient air for 25 days to have an overview on the changes of the surface state during the period of the experiment. The related bands or peaks in the IR spectra are introduced and corresponding vibration modes are assigned. Then, the oxidation kinetics is discussed based on the evolution of the IR spectra from 2.5 min to 25 days after HF etching. Finally, the correlation between the surface oxidation of the Si-NCs and the decrease of the electrical conductivity of our Si-NC films will be discussed.

6.1 Effect of HF Etching

The influence of the HF etching on the surface state of Si-NCs was studied by means of FT-IR spectroscopy. All the IR spectra were obtained in normal reflection mode at room temperature. Si-NCs were deposited directly on the reflection mirror, a gold layer thermally evaporated on the Kapton substrate. A Teflon holder was then glued under the Kapton piece for the convenience of HF etching. The sample was HF etched and stored in ambient condition. All FT-IR measurements were done in a vacuum chamber.

Figure 6.1 shows the FT-IR spectra from intrinsic Si-NCs before and after the HF treatment in the regions 700–1400 cm^{-1} and 1800–2400 cm^{-1}. Similar spectra (Fig. 6.1a

and b) have been reported in reference [1]. As can be seen in Fig. 6.1a, before HF etching, the spectrum is dominated by a broad band from 1000 to 1290 cm^{-1}, due to different stretching vibrations of Si-O-Si bonds arising from the surface oxide layer [3]. Besides, in the spectral range of the Si-H stretching and wagging modes, we observe peaks at 2254 and 880 cm^{-1} respectively, originating from Si-H bonds backbonded to three O atoms (O_3-Si-H unit) [4]. Additionally, a wide band centred at around 2115 cm^{-1} can also be seen, assigned to the Si-H stretching modes in various Si hydride configurations (Si_{4-n}-Si-H_n, n =1,2,3) [4].

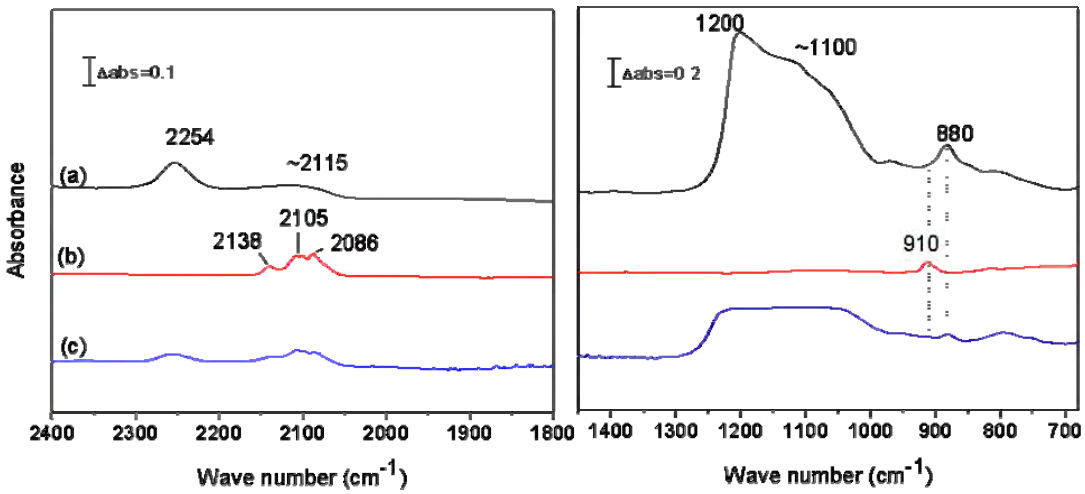

Fig. 6.1 Infrared absorbance spectra of the intrinsic Si-NC film (a) before HF etching; (b) 2.5 min and (c) 25 days exposure to air after HF etching.

The spectrum shown in Fig. 6.1b was measured with the HF etched film after 2.5 min of exposure to ambient condition after HF treatment. It can be seen that the bands at 2254 and ~1100 cm^{-1} related to the surface oxide are removed from the spectrum. The previous Si-H related band centred at around 2115cm^{-1} becomes structured and shows peaks at 2138 and 2086 cm^{-1} assigned to the symmetric and antisymmetric stretching modes of the Si-H in the di-hydride (Si_2-Si-H_2) configuration (Fig. 6.2), and a peak at 2105 cm^{-1} from the Si-H stretching in tri-hydride vibration (Si_3-Si-H) [4]. A contribution from the Si-H_2 scissors mode of the di-hydride (Si_2-Si-H_2) configuration is also observed at 910 cm^{-1} [4]. To summarize, the HF etching removes high potential barriers at the surface oxide layer of the Si-NCs, which strongly suppress the tunnelling of charge carriers between Si-NCs, and a predominant H-terminated surface of Si-NCs over the volume of the film is achieved. A

detailed review about the formation of the H-termination of the Si surface by HF etching may be obtained from reference [5].

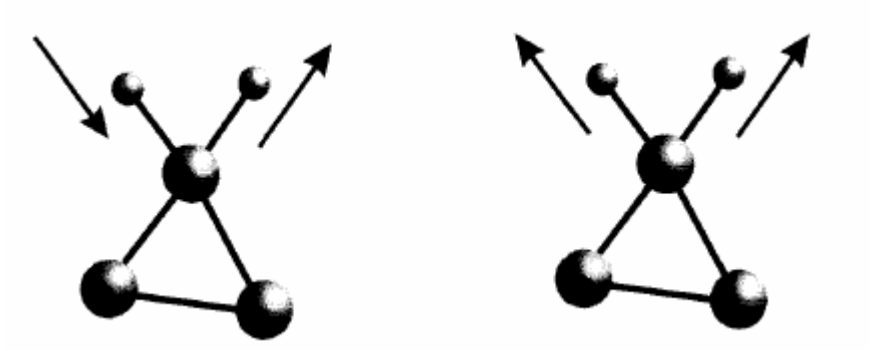

(a) antisymmetrical stretching (b) symmetrical stretching

Fig. 6.2 Stretching model of H atoms in the Si_2-Si-H_2 unit (big sphere: Si ; small sphere: H) [4]

After 25 days re-oxidation at ambient condition (Fig. 6.1c), the Si-O-Si broad band (~1100cm^{-1}) and the modes related to O_3-Si-H configuration (2254cm^{-1}) emerge again, whereas the Si-H_2 scissor mode (910cm^{-1}) decreases in intensity and the Si-H stretching modes from various Si hydride configurations (2138, 2105 and 2086cm^{-1}) show a tendency to merge into a broad band. Interestingly, the re-grown Si-O-Si broad band has a different shape from that observed before the HF treatment. This difference indicates changes on the oxide structure after HF etching and re-oxidation. Pi et al. suggest that HF etching leads to a decrease in the incorporation of O during subsequent oxidation, which finally results in sub-stoichiometric oxides (SiOx, X<2) [2]. However, their arguments are based on the observation that the peak of the Si-O-Si band shifts to a lower wave number (from 1074 to 1061 cm^{-1}). This can not be found in our study, since several bands overlap in this region complicating the analysis.

6.2 Oxidation Kinetics

Research on the oxidation behaviour of Si-NCs films is of interest because applications of Si-NC films in future technology demands a complete knowledge of the time dependent changes of Si-NC surface, simply in order to develop strategies for device processing. Oxidation of silicon surfaces involves the formation of an amorphous thin film on a crystalline surface. Two general steps can be divided: surface adsorption of “incoming”

oxygen atoms from ambient air and the incorporation of those atoms into silicon (bonds formation and surface reconstruction). Depending on the humidity of the air, periods of up to several months were found for the interfacial oxide growth on bulk Si [6] and porous Si [4]. In this work the oxidation of a HF etched intrinsic Si-NCs film is studied over a period of 25 days by monitoring the band region from 1300-850 cm^{-1} (Fig. 6.3 and Fig. 6.4) and 2400–1900 cm^{-1} (Fig. 6.5). As mentioned above, the first measurement after HF etching was carried out about 2.5 min after exposure to air, and then the spectra changes as a function of the exposure time at ambient condition were measured. Within the first hours of observation spectra have been recorded in intervals of 10-30 min, after that we used intervals of some hours and finally a weekly time scale was used. It should be mentioned that it was very important to investigate always one and the same sample spot in order to achieve comparable and consistent results.

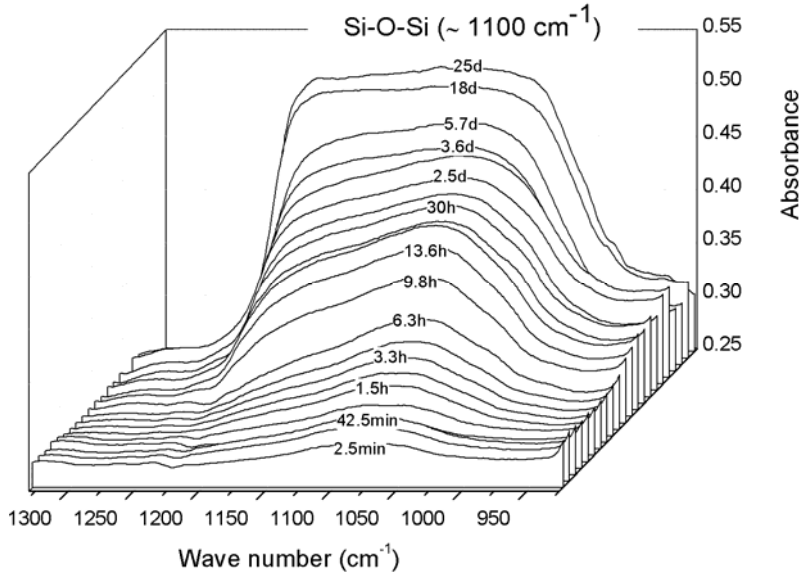

Fig. 6.3 Evolution of the IR band ranging from 1300 to 950 cm^{-1} in a period of 25 days exposure to air

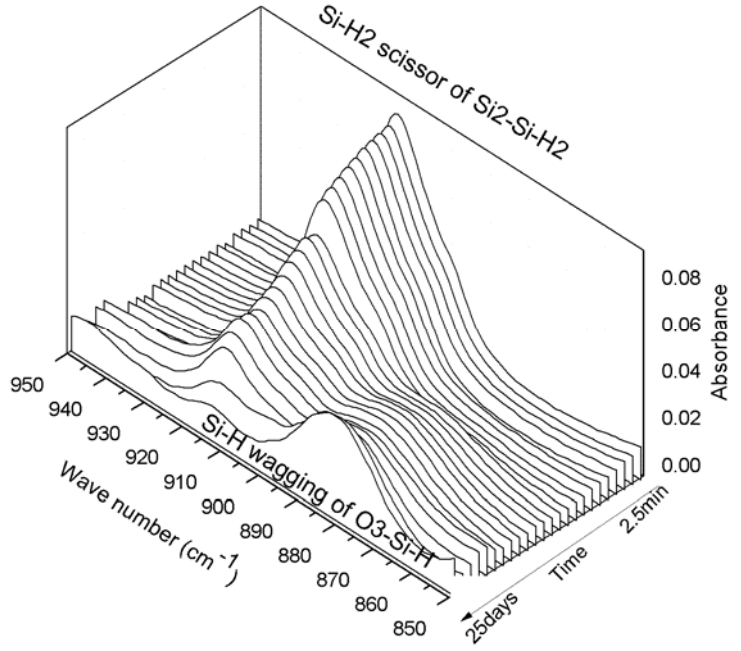

Fig. 6.4 Evolution of the IR band ranging from 950 to 850 cm^{-1} in a period of 25 days exposure to air. Intensity of the Si-H_2 scissor mode decreases gradually, whereas Si-H wagging from the O_3-Si-H unit grows

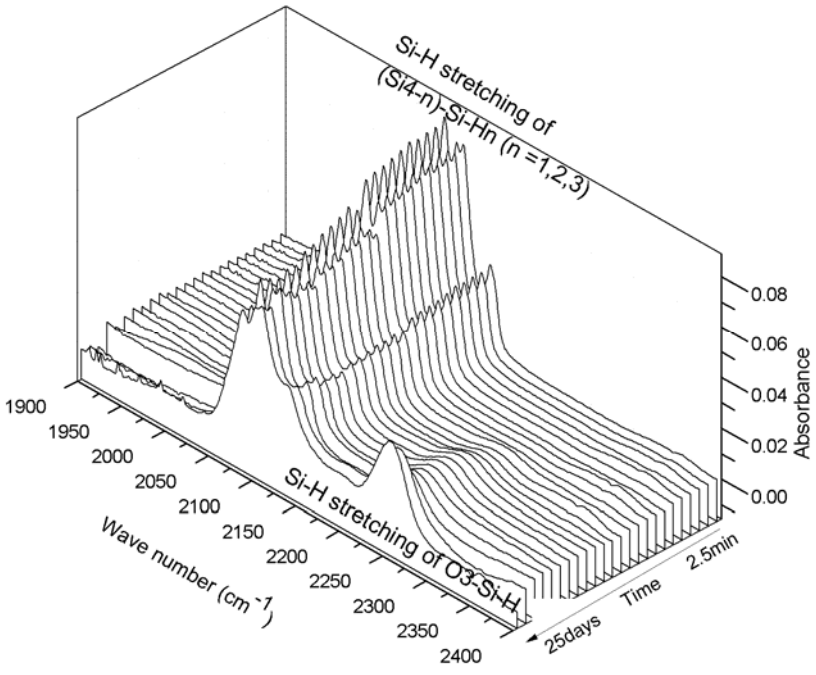

Fig. 6.5 Evolution of the IR band ranging from 2400 to 1900 cm^{-1} in a period of 25 days exposure to air. Intensity of the modes related with the hydrides configurations decreases gradually, whereas Si-H stretching mode from the O_3-Si-H unit increases.

It can be seen from Fig. 6.3 that the intensity of the Si-O-Si band increases and the band becomes broad with the exposure time to air after HF etching. During this period, the Si-H wagging (Fig. 6.4) and stretching (Fig. 6.5) modes from the O_3-Si-H unit increase, whereas the intensity of the Si-H stretching (Fig. 6.5) and the Si-H_2 scissor modes (Fig. 6.4) from Si_{4-n}-Si-H_n (n = 1, 2, 3) decrease. In order to quantify the spectra evolution, the changes in the strength of different vibration modes were estimated by the amplitude of the corresponding peaks. The results are plotted as a function of the exposure time in Fig. 6.6. It can be seen that the Si-O-Si band increases rapidly in the first 3 days, followed by a slower oxygen uptake. In the latter stage of our observation, a smaller growth of the Si-O-Si band can still be seen. Similar upward trends can be seen from the Si-H stretching (2254 cm^{-1}) and wagging modes (880 cm^{-1}) of the O_3-Si-H unit. On the contrary, the Si-H stretching (2086 cm^{-1}) and Si-H_2 scissor mode (910 cm^{-1}) from the Si_2-Si-H_2 configuration, which present prominent IR absorbance right after HF etching, show a fast decay in the initial 3 days and then slower decrease with the exposure time.

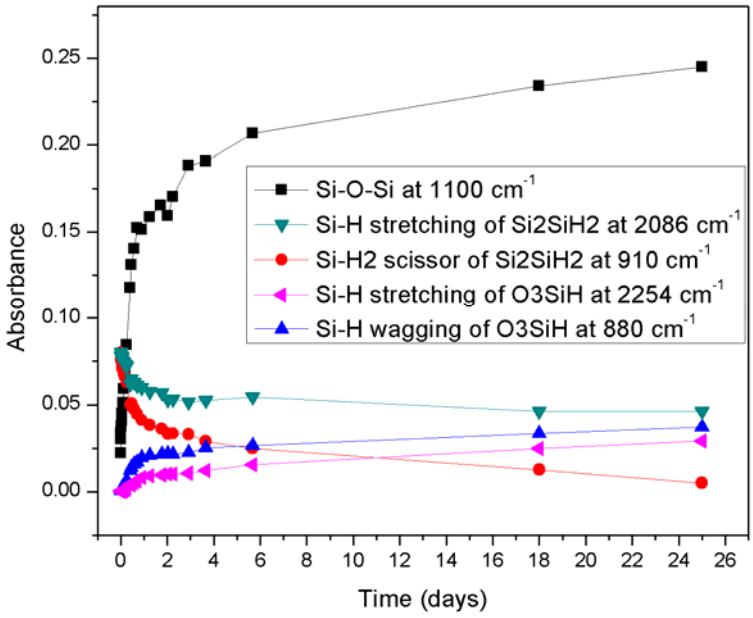

Fig. 6.6 Changes of several vibration modes as a function of the exposure time after HF etching

The oxidation mechanism of Si materials is controversial and several models have been suggested, including oxidation of the Si-H bonds with participation of water molecule [7], insertion of the O into the Si-Si backbonds [4] or by the termination of the Si-dbs [8]. According to reference [4], the oxidation of Si-Si backbonds is kinetically facilitated and

energetically favourable than breaking the relatively stable Si-H bonds. In our case, the growth of the bands related to the O_3-Si-H unit indicates that the oxidation of the Si-Si backbonds (as illustrated in Fig. 6.7) is involved in the oxidation procedure. This mechanism also contributes to the growth of the Si-O-Si bands and reduces the intensity of the bands from the hydride units Si_{4-n}-Si-H_n (n = 1, 2, 3). However, the oxidation of the back bonds is limited by the diffusion process that the oxygen atoms need to diffuse through the oxide layer. It is suggested that the activation energy of oxidant diffusivity increases in a highly stressed oxide, resulting in decrease of the oxidation rate [9]. The self-limited diffusion process may explain the smaller changes of all the bands during the latter period of our observation.

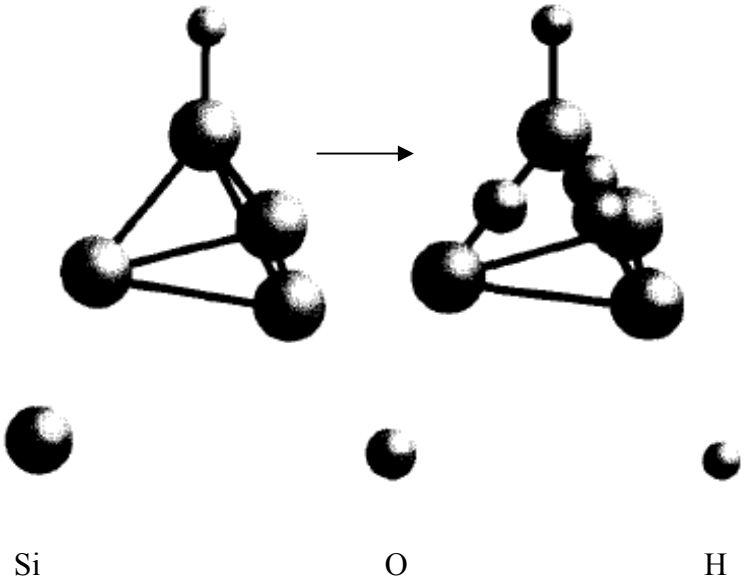

Fig. 6.7 Insertion of the O atom into the Si-Si back bonds [4] in the mono-hydride configuration

6.3 Correlation: Oxidation Behaviour and Electrical Properties

Figure 6.8 compares the evolution of the intensity of the Si-O-Si vibration mode at ~1100 cm^{-1} measured for our intrinsic Si-NCs, with the decrease in conductivity observed for the HF-etched film of also intrinsic Si-NCs after exposure to ambient conditions, over a period of 25 days. It can be seen that the conductivity degradation agrees well with the surface oxide growth. The oxide grows quickly in the first 3 days and correspondingly the

conductivity show a fast decay. The increase of the band intensity is slower after 3 days exposure to air, and the conductivity degrades also slower. This demonstrates that the decrease of the electrical conductivity of the HF-etched films can be mainly attributed to the growth of the surface oxide in air. Moreover, the good correlation between oxide growth and conductivity decrease also supports the above suggestion that the mechanism of electron transport in HF-etched films involves movement of charge carriers (e.g. tunnelling) between the Si-NC cores. The intrinsic Si-NCs are not fully oxidized in a period of 25 days exposure to air and corresponding conductivity degradation of the HF-etched film is also not saturated. Additionally, it is worth to point out that, other than the FT-IR spectroscopy, the electrical measurement may provide another approach to monitor the surface oxide growth of Si-NCs for the future work.

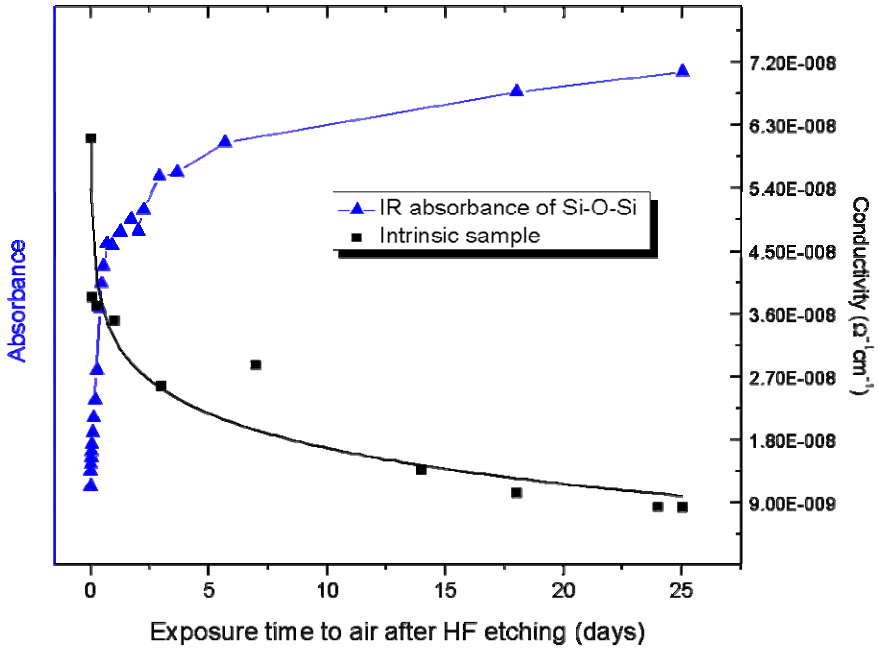

Fig. 6.8 Growth of the Si-O-Si band in the IR spectrum of intrinsic Si-NCs and the corresponding decrease in conductivity observed for the intrinsic Si-NC films, in a period of 25 days exposure to air after HF etching. The solid lines are guides to the eyes

6.4 References

[1] A.R. Stegner, R.N. Pereira, K. Klein, et al., Phys. Rev. Lett. 100 (2008) 026803.

[2] X.D. Pi, L. Mangolini, S.A. Campbell, et al., Phys. Rev. B. 75 (2007) 085423.

[3] C.T. Kirk, Phys. Rev. B 38 (1988) 1255.

[4] W. Theiss, Surf. Sci. Rep. 29 (1997) 95.
[5] Y.J. Chabal and K. Raghavachari, Surf. Sci. 502-503 (2002) 41.
[6] N. Herbots, J.M. Shaw, Q.B. Hurst, et al., Mater. Sci. Eng. B 87 (2001) 303.
[7] M. Niwano, J. Kageyama, K. Kurita, et al., J. Appt. Phys. 76 (1994) 4.
[8] T. Miura, M. Niwano, D. Shoji, et al., Appl. Surf. Sci. 100/101 (1996) 454.
[9] H.I. Liu, D.K. Biegelsen, N.M. Johnson, et al., Appl. Phys. Lett. 64 (1994) 1385.

7 Conclusion and Outlook

7.1 Conclusion

Si-NC films deposited onto flexible substrates by using Si inks are promising to be applied in cost efficient and versatile devices, such as detectors and thermoelectric devices. Investigation on the assembling and electrical behaviour of these nanocrystal networks is fundamental for their potential applications in the future.

In this work, Si-NCs grown from gas phase are dispersed in ethanol to prepare Si inks. The resulting inks are then spin coated onto Kapton substrates to form films of stacked Si-NCs. The influence of various processing parameters on the film thickness and morphology has been studied. As expected, the film thickness increases with the ink concentration and decreases with the spin rate in the spin coating process. As to the film morphology, a porous microstructure constituted by spherical Si-NCs was observed. Diluted Si inks (1.92 wt.%) produce films with poor coverage over the substrate, whereas concentrated Si inks (7.62 wt.%) result in films with many agglomerates of Si-NCs. The films produced from inks with concentration of ~5 wt.% show a good coverage over the substrate and a relative homogenous distribution of Si-NCs. Besides, we find that films produced from ball milled Si inks have less Si-NC agglomerates on the film surface than from the ultrasonic dispersed inks. Moreover, we observe that after the HF etching procedure, the Si-NC films become more densely packed, and their thickness decreases.

The macroscopic electrical behaviour has been investigated at ambient conditions. The effects of the Si-NC surface treatment (HF etching of Si-NCs), the electronic doping with phosphorus, the dispersion method of Si inks, and illumination on the electrical properties have been studied. We find that the σ-t curves of the Si-NC films measured at ambient condition show a fast decay caused by the applied voltage, followed by saturation at lower levels. The conductivity of intrinsic Si-NC films saturates at about $2\times10^{-9}\ \Omega^{-1}cm^{-1}$. A power-law dependence ($I\sim V^m$, with m = 1.68) is obtained as to the I-V behaviour of intrinsic Si-NC films. Neither the light exposure nor the P-doping leads to significant changes on the σ-t behaviour of Si-NC films.

HF etching is applied to remove the native oxide of Si-NCs. It is found that the conductivity of intrinsic Si-NC films increases to around 3×10^{-7} $\Omega^{-1}cm^{-1}$ after this treatment. The HF etched intrinsic Si-NC films also show an $I\sim V^m$ dependence (with m = 3.15). Moreover, an enhancement of the conductivity by illumination and P-doping can be seen after the HF treatment, which indicates that the conduction in Si-NC films is dominated by different mechanisms before and after the HF etching procedure. Additionally, we find that the films prepared from ultrasonic dispersed and ball milled Si inks show similar conductivity levels and σ-t curves both before and after the HF treatment.

After exposure to air, the HF etched films (both intrinsic and P-doped) show a degradation of conductivity over time: A rapid decay can be seen in the first three days, followed by a slow decrease.

The FT-IR measurements were further carried out to monitor changes in the surface state of Si-NCs and its evolution over time after removal of the native oxide layer by the HF etching treatment. We find that the HF etching removes the surface oxide of Si-NCs, resulting in a H-passivated surface. After exposed to air, the oxide grows fast in the initial three days, followed by a slow oxygen uptake. During the period (25 days) of our observation, the Si-NCs were not fully oxidized. The oxidation of Si-Si backbonds is considered to contribute to the oxide growth. Interestingly, the time dependence of ambient oxidation of Si-NCs agrees very well with that of the decrease of the conductivity of the HF-etched films over time, which demonstrates that the decrease of the electrical conductivity of the Si-NC films after HF etching can be mainly attributed to the growth of the surface oxide in air.

7.2 Future work

More work can be done in the future, discussed as follows.

1. Prevent oxidation after the HF treatment

As concluded above, the oxidation of Si-NCs after HF etching degrades the electrical conductivity. Further research is necessary to develop strategies to avoid the fast decay of the conductivity when the "clean" surface of Si-NCs exposed to ambient air. A suggestion would be to coat the Si-NCs with an oxidation resistant layer.

2. Further characterizations

Further electrical measurements can be done with well controlled measurement conditions, for example, the gas environment or the local temperature of the films. Besides, the photo-current of the Si-NC films can be measured, to further study the conduction mechanism of Si-NC films before and after HF etching.

3. Improve the fabrication process

The film quality can be improved by optimizing the process. For example, the film density might be enhanced by multi-layer coating process. Besides, the HF etching treatment can be done in a HF vapour to reduce or even avoid loss of Si-NCs in the films.